Spin-orbit-coupled Bose-Einstein condensates in a cavity: Route to magnetic phases through cavity transmission

Bikash Padhi and Sankalpa Ghosh*
Department of Physics, IIT Delhi, New Delhi 110016, India
(Received 17 May 2014; published 20 August 2014)

We study the spin-orbit-coupled ultracold Bose-Einstein condensate placed in a single-mode Fabry-Pérot cavity. The cavity introduces a quantum optical lattice potential which dynamically couples with the atomic degrees of freedom and realizes a generalized modified Bose-Hubbard model whose zero-temperature phase diagram can be controlled by tuning the cavity parameters. In the noninteracting limit, where the atom-atom interaction is set to 0, the resulting atomic dispersion shows interesting features such as a bosonic analog of Dirac points, a cavity-controlled Hofstadter spectrum which bears the hallmark of pseudospin-1/2 bosons in the presence of Abelian and non-Abelian gauge fields (the latter due to spin-orbit coupling) in a cavity-induced optical lattice potential. In the presence of atom-atom interaction, using a mapping to a generalized Bose-Hubbard model of spin-orbit-coupled bosons in a classical optical lattice, we show that the system realizes a host of quantum magnetic phases whose magnetic order can be detected from the cavity transmission. This provides an alternative approach to detecting quantum magnetism in ultracold atoms. We discuss the effects of cavity-induced optical bistability on these phases and their experimental consequences.

DOI: 10.1103/PhysRevA.90.023627 PACS number(s): 03.75.Mn, 42.50.Pq, 32.10.Fn, 33.60.+q

I. INTRODUCTION

Quantum simulation of exotic condensed matter phases [1–3] with ultracold atoms has witnessed tremendous progress in recent times. A significant step in the direction of realization of such exotic phases was taken through the experimental realization of synthetic spin-orbit coupling for bosonic ultracold systems [4,5] and, subsequently, for fermionic ultracold atoms [6,7]. The development opened the possibility of simulating analogs of topologically nontrivial condensed matter phases [8], as well as quantum magnetic phases [9] in the domain of ultracold atoms. All these developments led to a flurry of theoretical as well as experimental activity in this direction [10].

In this work we consider such spin-orbit-coupled (SOC) ultracold Bose-Einstein condensate (BEC) inside a Fabry-Pérot cavity (see Fig. 1) and study the consequences of atom-photon interaction on the phase diagram of SOC bosons. The motivation for studying SOC ultracold atoms in this unique environment comes from the recent progress in studying ultracold atomic systems in a high-finesse single-mode optical cavity [11–17] and the resulting cavity optomechanics with ultracold atoms. The presence of an atomic ensemble in the form of a BEC in such an optical cavity allows a strong optomechanical coupling between the collective mode of the condensate and the photon field. Consequently the quantum many-body state of the atom can be probed by analyzing the cavity transmission. The coupled atom-photon dynamics, resulting backaction, cavity-induced bistability—all these together can lead to a number of interesting phenomena including self-organization of the atomic many body states [18–21] and bistability-induced quantum phase transition [22].

In this context, the deliberated quantum optics with an SOC BEC in a high-finesse Fabry-Pérot cavity that forms the subject matter of the current work is interesting on more than one account. First, the cavity-atom interaction provides a dynamic optical lattice potential [23] for the SOC Bose gas where the optical lattice potential is dynamically altered through its interaction with the ultracold atomic condensate inside. This allows one to realize certain variants of the modified Bose-Hubbard model (mBHM). Thus far, following the seminal work on the superfluid (SF)–Mott insulator (MI) transition in ultracold atoms [24,25], the mBHM has been studied mostly in the presence of the prototype classical optical lattice potential. However, now the dynamical nature of the photon field contributes additional features and profoundly influences the resulting phase diagram.

It has been shown in the recent literature [26–29] that a number of intriguing quantum magnetic phases can be realized by such ultracold SOC Bose-Einstein systems in a classical optical lattice potential. Our study of such SOC BECs inside a cavity clearly analyzes such magnetic orders when the photon field is treated dynamically and clearly demonstrates how such magnetic phases can be detected by analyzing the transmission of photons from the cavity. As we point out, this provides an alternative way of detecting quantum magnetic phases of ultracold atoms. The cavity spectrum can be used to detect various other properties of cold atomic systems such as the MI-SF transition [16], detection of Landau levels in fermionic systems [30], phase diagram of a two-component Bose gas [31], and many more [11]. It was also proposed to create a synthetic spin-orbit interaction in a ring-cavity system [32].

The spin-orbit coupling also realizes a synthetic non-Abelian gauge field for such an ultracold atomic system [4,33], and consequently, a spin-1/2 Bose system is also realized (we use "spin" and "pseudospin" interchangeably), which is fundamentally prevented by the spin-statistics theorem [10,34]. Our theoretical framework allows us to study the single-atom spectrum of such an esoteric quantum system in the environment of a dynamical optical lattice induced by the cavity and brings out the intriguing properties of the resulting band structure.

*sankalpa@physics.iitd.ac.in

The sequence of subsequent discussion is as follows. The SOC Bose system we consider here was motivated by a recent experiment by the NIST group [4]. In Sec. II we begin by introducing the fully second-quantized Hamiltonian of such systems inside a single-mode optical cavity in terms of the annihilation and creation operators of photons and atoms. The Hamiltonian and the resulting Heisenberg equation of motion of the field operators clearly demonstrate the dynamical nature of the optical lattice. Adiabatically eliminating the exited states of the atomic condensate we obtain an effective Hamiltonian for pseudo-spin-1/2 Bose-Einstein systems where the pseudospin degrees of freedom corresponds to the two lowest hyperfine states of the original multiplet of the ultracold atomic system considered. In the subsequent discussion, using a tight-binding approximation we derive the mBHM for the resulting system. We show that this can be mapped suitably to the Bose-Hubbard model (BHM) of an SOC Bose gas in a classical optical lattice created by standing waves of counterpropagating laser beams [26]. But now the lattice parameters are being controlled by the cavity parameters as well as atom-photon interaction.

We arrive at our final Hamiltonian [Eq. (26)] in Sec. III A, which is an mBHM. In the subsequent Sec. III B, we study the energy spectrum of this mBHM in the limit where the atom-atom interaction vanishes. In the presence of an optical lattice and synthetic non-Abelian gauge field created by the spin-orbit coupling, the system shows a highly intriguing band structure that features the existence of Dirac points in such a bosonic system like their fermionic counterpart, a property which underscores the spin 1/2 of this bosonic system. Then in Sec. III C we discuss the various magnetic phases stabilized by the ground state of this Hamiltonian. We consider such magnetic phases in a deep optical lattice regime where the orbital part is always an MI state and the spinorial part can realize various magnetic phases through its texturing.

In Sec. IV we study the probing method, i.e., how to detect various magnetic phases in an MI type of ground state through the cavity transmission spectrum. Our suggestion provides an alternative way of detecting quantum magnetism in ultracold atomic systems. The role of cavity-induced bistability in the detection of such magnetic phases and the related phase transition are also discussed. We, finally, discuss the possibility of experimental realization of our scheme and conclude in Sec. V.

II. THE MODEL

We consider a condensate of N_0 ^{87}Rb atoms in two internal states, $|m_F\rangle = |1\rangle,|0\rangle$, available in the $F = 1$ manifold of the $5S^{1/2}$ electronic levels (see Fig. 1). These two states are coupled by a pair of suitably detuned Raman lasers, and a combination of Rashba and Dresselhaus spin-orbit coupling is realized [4]. This SOC BEC is now coherently driven into a linear cavity by a strong far-off resonant pump laser, where it interacts with a single mode of the cavity. We consider a high-Q cavity (i.e., a cavity in which a photon takes a large number of round trips before it leaks out) with a strong atom-field coupling. Not only do these two considerations enhance the atom-photon dipole interaction, but also the backaction of the atoms on the light becomes significant [12–14]. The resulting atom-cavity interaction thus generates

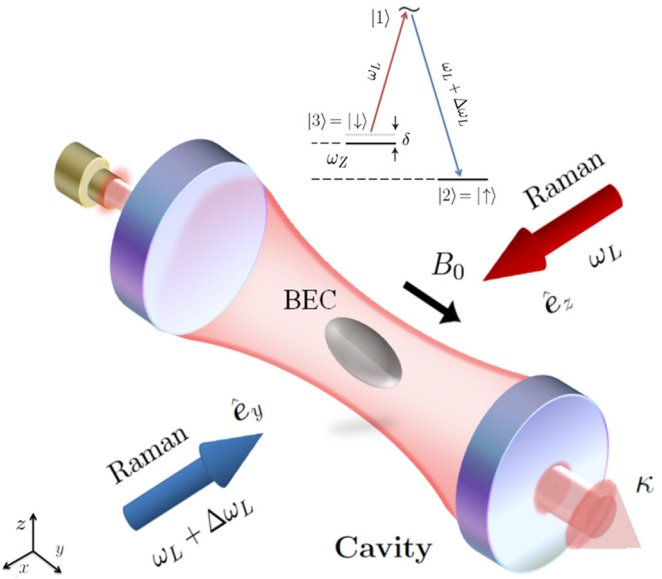

FIG. 1. (Color online) ^{87}Rb BEC inside an optical cavity: SOC is created by two counterpropagating Raman lasers with frequencies ω_L and $\omega_L + \Delta\omega_L$ that are applied along $\hat{x}$. The Raman beams are polarized along $\hat{z}$ and $\hat{y}$ (gravity is along $-\hat{z}$). A bias field B_0 is applied along $\hat{y}$ to generate the Zeeman shift. Inset: Level diagram of the ^{87}Rb atom. Internal states are denoted $|1\rangle,|2\rangle,|3\rangle$. The coupling of these states is shown schematically.

a two-dimensional (2D) square optical lattice potential which is now dynamical [11,23].

A. The single-particle Hamiltonian

We derive the single-particle Hamiltonian for a two-component BEC interacting with a strong, classical pump field and a weak, quantized probe field. Assuming a dipole-like interaction and using the rotating-wave approximation we can describe a single atom of this system by the Jaynes-Cummings-like Hamiltonian [35]

$$\hat{H} = \hat{H}_A + \hat{H}_C + \hat{H}_I. \tag{1}$$

Denoting the atomic transition frequencies ω_{ij} and the transition operator $\hat{\xi}_{ij} = |i\rangle\langle j|$, we express the atomic ($\hat{H}_A$), cavity ($\hat{H}_C$), and atom-cavity interaction ($\hat{H}_I$) Hamiltonians as

$$\hat{H}_A = \frac{\hat{\mathbf{\Pi}}^2}{2m} + \hbar\omega_{12}\hat{\xi}_{11} + \hbar\omega_{13}\hat{\xi}_{11}, \tag{2a}$$

$$\hat{H}_C = \hbar\omega_c\hat{a}^\dagger\hat{a} - i\hbar\eta(\hat{a}e^{i\omega_p t} - \hat{a}^\dagger e^{-i\omega_p t}), \tag{2b}$$

$$\hat{H}_I = -i\hbar g(\boldsymbol{x})(\hat{\xi}_{12}\hat{a} - \hat{\xi}_{21}\hat{a}^\dagger + \hat{\xi}_{13}\hat{a} - \hat{\xi}_{31}\hat{a}^\dagger). \tag{2c}$$

Here $\hat{\mathbf{\Pi}}^2/2m = (\boldsymbol{p} + m\boldsymbol{A})^2/2m$ is the covariant momentum of the bosons. The synthetic vector potential $\boldsymbol{A}$ is taken to be of the form $\boldsymbol{A}_{U(1)} + A_{SU(2)}$, where the Abelian field is [36] $A_{U(1)} = (0, B_0 x, 0)$ and the spin-orbit-coupling-induced non-Abelian field is $\boldsymbol{A}_{SU(2)} = (\alpha\sigma_y, \beta\sigma_x, 0)$ which is [4] a combination of Rashba- and Dresselhouse [37]-type spin-orbit coupling. When $\beta = -\alpha$ the spin-orbit coupling is purely of the Rashba type. Here α and β actually denote the dimensionless SOC strength in units of $\frac{\hbar K}{\pi m}$, where K is the wave number corresponding to the cavity photon. $\hat{\sigma}_{x,y,z}$

are 2×2 spin-1/2 representations of Pauli matrices. η is the coupling between the pump and the cavity, ω_p is the frequency of the pump laser, which we set to be $\omega_L + \Delta\omega_L$, ω_c is the frequency of the cavity photon, which is almost in resonance with the pump beam, and $\Delta_c = \omega_p - \omega_c = \Delta\omega_L \approx \kappa$, with 2κ being the cavity decay line width. The operator $\hat{a}$ ($\hat{a}^\dagger$) annihilates (creates) one cavity photon.

$g^2(\boldsymbol{x})$ is the cavity mode function, which varies as the spatial mode profile, and we take $g^2(\boldsymbol{x}) = g_0[\cos^2(Kx) + \cos^2(Ky)]$, where g_0 is the coupling strength of the atom and cavity field. We also assume that the wave vectors along x and y directions are the same, namely, $K_x = K_y = K$. For simplicity, we assume that both transitions, $|2\rangle \leftrightarrow |1\rangle$ and $|3\rangle \leftrightarrow |1\rangle$, have the same coupling with the cavity. Assuming the atoms to be in the same motional quantum state, the coupling g_0 is assumed to be identical for all atoms. In order to remove the time dependence of the above Hamiltonian we perform a unitary transformation on the above Hamiltonian with $\hat{U}(t) = \exp[i\omega_p t(\hat{\xi}_{11} + \hat{a}^\dagger\hat{a})]$ [38]. The purpose of this unitary transformation is to describe the system in terms of slowly changing variables. In Appendix A 2 we explain in detail the results derived from the transformed Hamiltonian below, which will also remain valid in the laboratory frame, provided that the time scale associated with atomic dynamics is much faster in comparison with the time scale associated with the pump laser frequency, $\sim 1/\omega_p$.

Using Baker's lemma the following Hamiltonians are obtained (see Appendix A 1):

$$\hat{H}_A = \frac{\hat{\mathbf{\Pi}}^2}{2m} - \hbar\Delta^a_{12}\hat{\xi}_{11} - \hbar\Delta^a_{13}\hat{\xi}_{11}, \tag{3a}$$

$$\hat{H}_C = -\hbar\Delta_c\hat{a}^\dagger\hat{a} - i\hbar\eta(\hat{a} - \hat{a}^\dagger) + \kappa\hat{a}^\dagger\hat{a}, \tag{3b}$$

$$\hat{H}_I = -i\hbar g(\boldsymbol{x})(\hat{\xi}_{12}\hat{a} - \hat{\xi}_{21}\hat{a}^\dagger + \hat{\xi}_{13}\hat{a} - \hat{\xi}_{31}\hat{a}^\dagger). \tag{3c}$$

The atom-pump detuning is denoted $\Delta^a_{ij} = \omega_p - \omega_{ij}$. Henceforth we denote $\Delta_a = \Delta^a_{12} + \Delta^a_{13}$. The extra term $\kappa\hat{a}^\dagger\hat{a}$ appearing in $\hat{H}_C$ can be justified in the following way: in the presence of external pumping of atoms the system becomes an open quantum system and hence dissipation effects must be incorporated. This is done using the master equation approach for (atom-field) density matrices [16,39]. Thus the effect of photon loss due to cavity decay line width (κ) gets incorporated.

B. The many-body Hamiltonian

Following Refs. [16,22] and [38] we now derive the full many-body Hamiltonian for this system. To do so we construct a matrix of all the transition operators and project it onto a full many-body space. This causes the transition operator $\hat{\xi}_{ij}$ to pick up the product of $\hat{\Psi}^\dagger_i$ and $\hat{\Psi}_j$. So the final form of the many-body Hamiltonian becomes

$$\hat{\mathcal{H}}_A = \int d\boldsymbol{x}\left[\hat{\Psi}^\dagger_2(\boldsymbol{x})\left(\frac{\hat{\mathbf{\Pi}}^2}{2m}\right)\hat{\Psi}_2(\boldsymbol{x}) + \hat{\Psi}^\dagger_3(\boldsymbol{x})\left(\frac{\hat{\mathbf{\Pi}}^2}{2m}\right)\hat{\Psi}_3(\boldsymbol{x}) + \hat{\Psi}^\dagger_1(\boldsymbol{x})\left(\frac{\hat{\Pi}^2}{2m} - \hbar\Delta_a\right)\hat{\Psi}_1(\boldsymbol{x})\right]. \tag{4}$$

Here $\hat{\Psi}_i(\boldsymbol{x})$ and $\hat{\Psi}^\dagger_i(\boldsymbol{x})$ are the annihilation and creation operators for an atom at position $\boldsymbol{x}$ in spin state $|i\rangle$. They obey the usual bosonic commutation relations:

$$[\hat{\Psi}_i(\boldsymbol{x}), \hat{\Psi}^\dagger_j(\boldsymbol{x}')] = \delta^3(\boldsymbol{x} - \boldsymbol{x}')\delta_{ij}, \tag{5a}$$

$$[\hat{\Psi}_i(\boldsymbol{x}), \hat{\Psi}_j(\boldsymbol{x}')] = [\hat{\Psi}^\dagger_i(\boldsymbol{x}), \hat{\Psi}^\dagger_j(\boldsymbol{x}')] = 0. \tag{5b}$$

Since the cavity-field operators commute with the atomic operators the Hamiltonian $\hat{\mathcal{H}}_C$ remains unchanged in the second-quantized notation. In our analysis we assume that the pump mode is chosen so that its interaction with the atoms is solely along the $\hat{z}$ axis, allowing us to exclude its dynamics on the x-y plane. The two-body interaction between atoms in the same and different spin states is modeled through [4]

$$\hat{\mathcal{H}}_U = \frac{U}{2}\int d\boldsymbol{x}[\hat{\Psi}^\dagger_2(\boldsymbol{x})\hat{\Psi}^\dagger_2(\boldsymbol{x})\hat{\Psi}_2(\boldsymbol{x})\hat{\Psi}_2(\boldsymbol{x}) + \hat{\Psi}^\dagger_3(\boldsymbol{x})\hat{\Psi}^\dagger_3(\boldsymbol{x})\hat{\Psi}_3(\boldsymbol{x})\hat{\Psi}_3(\boldsymbol{x}) + \lambda\hat{\Psi}^\dagger_2(\boldsymbol{x})\hat{\Psi}^\dagger_3(\boldsymbol{x})\hat{\Psi}_2(\boldsymbol{x})\hat{\Psi}_3(\boldsymbol{x})], \tag{6}$$

where the intraspecies interaction strength is measured by $U = 4\pi a_s^2\hbar^2/m$ and the interspecies interaction is measured by λU, where the parameter λ is decided by the laser configuration. Here a_s is the s-wave scattering length. Next, the many-body interaction between the atom and the cavity can be modeled as

$$\hat{\mathcal{H}}_I = -i\hbar\int d\boldsymbol{x}[\hat{\Psi}^\dagger_1(\boldsymbol{x})\hat{a}\hat{\Psi}_2(\boldsymbol{x}) + \hat{\Psi}^\dagger_1(\boldsymbol{x})\hat{a}\hat{\Psi}_3(\boldsymbol{x}) + \text{H.c.}]g(\boldsymbol{x}). \tag{7}$$

Now we calculate the Heisenberg equations of evolution for various field operators (say $\hat{A}$), $i\hbar\partial_t\hat{A} = [\hat{A}, \hat{\mathcal{H}}]$, yielding

$$\frac{\partial\hat{\Psi}_1(\boldsymbol{x})}{\partial t} = -i\left(\frac{\hat{\mathbf{\Pi}}^2}{2\hbar m} - \Delta_a\right)\hat{\Psi}_1(\boldsymbol{x}) - g(\boldsymbol{x})\hat{a}[\hat{\Psi}_2(\boldsymbol{x}) + \hat{\Psi}_3(\boldsymbol{x})], \tag{8a}$$

$$\frac{\partial\hat{\Psi}_2(\boldsymbol{x})}{\partial t} = -i\left[\frac{\hat{\mathbf{\Pi}}^2}{2\hbar m} + \frac{U}{\hbar}\hat{\Psi}^\dagger_2(\boldsymbol{x})\hat{\Psi}_2(\boldsymbol{x}) + \frac{U\lambda}{\hbar}\hat{\Psi}^\dagger_3(\boldsymbol{x})\hat{\Psi}_3(\boldsymbol{x})\right]\times\hat{\Psi}_2(\boldsymbol{x}) + g(\boldsymbol{x})\hat{a}^\dagger\hat{\Psi}_1(\boldsymbol{x}), \tag{8b}$$

$$\frac{\partial\hat{\Psi}_3(\boldsymbol{x})}{\partial t} = -i\left[\frac{\hat{\mathbf{\Pi}}^2}{2\hbar m} + \frac{U}{\hbar}\hat{\Psi}^\dagger_3(\boldsymbol{x})\hat{\Psi}_3(\boldsymbol{x}) + \frac{U\lambda}{\hbar}\hat{\Psi}^\dagger_2(\boldsymbol{x})\hat{\Psi}_2(\boldsymbol{x})\right]\times\hat{\Psi}_3(\boldsymbol{x}) + g(\boldsymbol{x})\hat{a}^\dagger\hat{\Psi}_1(\boldsymbol{x}), \tag{8c}$$

$$\frac{\partial\hat{a}(t)}{\partial t} = i\Delta_c\hat{a}(t) + \eta + \int d\boldsymbol{x}[\hat{\Psi}^\dagger_2(\boldsymbol{x})g(\boldsymbol{x})\hat{\Psi}_1(\boldsymbol{x}) + \hat{\Psi}^\dagger_3(\boldsymbol{x})g(\boldsymbol{x})\hat{\Psi}_1(\boldsymbol{x})]. \tag{8d}$$

In the evolution of atomic operators the first term describes the free evolution of the atomic states. In (8a) the second term describes the absorption of a cavity photon by an atom, causing an excitation from $|2\rangle$ or $|3\rangle$ to the excited state $|1\rangle$. Similarly in (8b) or (8c) the second term describes the emission of a cavity photon followed by the relaxation of an atom from state $|1\rangle$ to state $|2\rangle$ or $|3\rangle$. The first term in (8d) is the free evolution term and the last two terms are the two additional driving terms

of the field, one by the pump and the other by the emission of an atom due to relaxation from state $|1\rangle$ to state $|2\rangle$ or $|3\rangle$.

In order to preserve the BEC in its ground state we must avoid heating, primarily caused by spontaneous emission from the atoms. The excited state varies at a time scale of $1/\gamma$ (atomic line width) and the ground state and cavity photons evolve at a time scale of $1/\Delta_a$. Hence by choosing a large atom-pump detuning, $\Delta^a_{ij} \gg \gamma$, we can adiabatically eliminate the excited states from the dynamics of our system [16,38]. By setting $\partial_t \hat{\Psi}_1(\boldsymbol{x}) = 0$ we obtain

$$\hat{\Psi}_1(\boldsymbol{x}) = -\frac{i}{\Delta_a} g(\boldsymbol{x}) \hat{a}(t)[\hat{\Psi}_2(\boldsymbol{x}) + \hat{\Psi}_3(\boldsymbol{x})]. \tag{9}$$

Inserting this into (8) we get

$$\frac{\partial \hat{\Psi}_2(\boldsymbol{x})}{\partial t} = -i\Bigg[\frac{\hat{\boldsymbol{\Pi}}^2}{2\hbar m} + \frac{U}{\hbar}\hat{\Psi}_2^\dagger(\boldsymbol{x})\hat{\Psi}_2(\boldsymbol{x}) + \frac{U\lambda}{\hbar}\hat{\Psi}_3^\dagger(\boldsymbol{x})\hat{\Psi}_3(\boldsymbol{x}) + \frac{g^2(\boldsymbol{x})}{\Delta_a}\hat{a}^\dagger\hat{a}\Bigg]\hat{\Psi}_2(\boldsymbol{x}) - i\frac{g^2(\boldsymbol{x})}{\Delta_a}\hat{a}^\dagger\hat{a}\hat{\Psi}_3(\boldsymbol{x}), \tag{10a}$$

$$\frac{\partial \hat{\Psi}_3(\boldsymbol{x})}{\partial t} = -i\Bigg[\frac{\hat{\boldsymbol{\Pi}}^2}{2\hbar m} + \frac{U}{\hbar}\hat{\Psi}_2^\dagger(\boldsymbol{x})\hat{\Psi}_2(\boldsymbol{x}) + \frac{U\lambda}{\hbar}\hat{\Psi}_3^\dagger(\boldsymbol{x})\hat{\Psi}_3(\boldsymbol{x}) + \frac{g^2(\boldsymbol{x})}{\Delta_a}\hat{a}^\dagger\hat{a}\Bigg]\hat{\Psi}_3(\boldsymbol{x}) - i\frac{g^2(\boldsymbol{x})}{\Delta_a}\hat{a}^\dagger\hat{a}\hat{\Psi}_2(\boldsymbol{x}), \tag{10b}$$

$$\frac{\partial a(t)}{\partial t} = i\Bigg[\Delta_c - \frac{1}{\Delta_a}\int d\boldsymbol{x}\, g^2(\boldsymbol{x})[\hat{\Psi}_2^\dagger(\boldsymbol{x})\hat{\Psi}_2(\boldsymbol{x}) + \hat{\Psi}_3^\dagger(\boldsymbol{x})\hat{\Psi}_3(\boldsymbol{x}) + \hat{\Psi}_2^\dagger(\boldsymbol{x})\hat{\Psi}_3(\boldsymbol{x}) + \hat{\Psi}_3^\dagger(\boldsymbol{x})\hat{\Psi}_2(\boldsymbol{x})]\Bigg]\hat{a} + \eta. \tag{10c}$$

This set of equations is characteristic of a cavity optomechanical system [40]. Here we have developed them specifically for an SOC BEC system. Since we have adiabatically eliminated the excited state $|1\rangle$ from the dynamics, henceforth we drop the notation {2,3}, and use $\{\uparrow,\downarrow\}$ instead, to use the language of "pseudospins." In other words, the two laser-dressed hyperfine states $|F = 1, m_F = 0\rangle$ and $|F = 1, m_F = 1\rangle$ of the ^{87}Rb atoms are now mapped to a synthetic spin-1/2 system (hence pseudospin), with states labeleds $|\uparrow\rangle$ and $|\downarrow\rangle$. It must be noted that there exist no real spin-1/2 bosonic systems in nature due to spin-statistics theorem, but with the help of lasers we could realize such a system in an ultracold atomic condensate [4]. In later sections we show how this strange property of the system leads to some interesting results which are unconventional in bosonic systems.

Now the dynamics of the atoms effectively comprises the dynamics of two-species (denoted by their pseudospin label) bosons coupled by a spin-orbit interaction. The effective Hamiltonian $\hat{\mathcal{H}}_{\text{eff}}$, which captures the effective dynamics of the system described in (10), $i\hbar\partial_t\hat{\Psi}_{\uparrow,\downarrow}(\boldsymbol{x}) = [\hat{\Psi}_{\uparrow,\downarrow}(\boldsymbol{x}), \hat{\mathcal{H}}_{\text{eff}}]$ and $i\hbar\partial_t\hat{a} = [\hat{a}, \hat{\mathcal{H}}_{\text{eff}}]$,

$$\hat{\mathcal{H}}^{(1)}_{\text{eff}} = \int d\boldsymbol{x}\,\hat{\boldsymbol{\Psi}}^\dagger(\boldsymbol{x})\left(\frac{\hat{\boldsymbol{\Pi}}^2}{2m} + U_{\text{lat}}\right)\hat{\boldsymbol{\Psi}}(\boldsymbol{x}) + \hat{H}_c + \frac{1}{2}\int d\boldsymbol{x}\sum_{s,s'} U_{s,s'}\hat{\Psi}_s^\dagger(\boldsymbol{x})\hat{\Psi}_{s'}^\dagger(\boldsymbol{x})\hat{\Psi}_{s'}(\boldsymbol{x})\hat{\Psi}_s(\boldsymbol{x}). \tag{11}$$

Here $s, s' \in \{\uparrow,\downarrow\}$. For simplification of the notation we have defined a column vector $\hat{\boldsymbol{\Psi}} = (\hat{\Psi}_\uparrow, \hat{\Psi}_\downarrow)^T$. The atom-atom interaction strength is denoted $U_{\uparrow,\uparrow} = U_{\uparrow,\uparrow} = U$ and $U_{\uparrow,\downarrow} = U_{\downarrow,\uparrow} = \lambda U$. One can note that the atom-cavity coupling has led to the formation of an optical lattice [38], which is $U_{\text{lat}} = V_0[\cos^2(Kx) + \cos^2(Ky)]$. Here V_0 is the depth of the well, $V_0 = \hbar U_0 \hat{a}^\dagger\hat{a}$, and $U_0 = g_0^2/\Delta_a$ is the effective atom-photon coupling strength. Now since the lattice depth has become a (photon number) operator, it is no longer a classical lattice, but a quantum lattice. In our calculations we have taken an Nd:Yag (green) laser source of $\lambda = 1064$ nm (hence the lattice constant is $a_0 = \lambda/2 = 532$ nm). The kinetic energy of an atom carrying 1 unit of photon momentum, $|\boldsymbol{p}| = \hbar K$, describes the characteristic frequency of the center-of-mass motion of the cloud. Thus the relevant energy scale is $E_r = \hbar^2K^2/2m$ (recoil energy), in the units in which we measure all other energies involved in the problem. For our case the lattice recoil frequency is $\omega_r = E_r/\hbar = 12.26$ kHz.

C. The modified Bose-Hubbard model

To investigate various interesting phases of this system through the cavity spectrum, first we establish an equivalence of the effective Hamiltonian obtained in (11) in a cavity-induced quantum optical lattice with a prototype BHM in a classical optical lattice. Using the tight-binding approximation this is done as follows. By constructing maximally localized eigenfunctions at each site on the lattice we expand each component of the atomic field operator $\hat{\Psi}_s$ in the basis of Wannier functions [41],

$$\hat{\Psi}_s(\boldsymbol{r}) = \sum_i \hat{b}_{si}\, w(\boldsymbol{r} - \boldsymbol{r}_i), \tag{12}$$

where $\hat{b}^\dagger_{si}$ is a bosonic operator that creates an atom in pseudospin state $|s\rangle$ ($s = \{\uparrow,\downarrow\}$) at site i on the optical lattice. However, in the presence of a gauge potential the Wannier functions pick up a gauge-dependent phase and should be modified as

$$w(\boldsymbol{r} - \boldsymbol{r}_i) \to W(\boldsymbol{r} - \boldsymbol{r}_i) = e^{-i\frac{m}{\hbar}\int_{r_i}^{r}\boldsymbol{A}(\boldsymbol{r}')\cdot d\boldsymbol{l}} w(\boldsymbol{r} - \boldsymbol{r}_i). \tag{13}$$

First, we show that under the nearest-neighbor approximation (i.e., hopping is permitted between two adjacent sites only), the gauge-transformed Wannier function in (13) forms a valid basis for the Hilbert space; then we expand the effective Hamiltonian in (11) in this basis. We denote $w(\boldsymbol{r} - \boldsymbol{r}_i)$ as $w_i(\boldsymbol{r})$. The norm of the gauge-transformed Wannier functions becomes equal to unity since the gauge transformation only introduces a phase factor. So we check for orthogonality only. The inner product is

$$\begin{aligned}\int d\boldsymbol{r}\, W_i^*(\boldsymbol{r})W_j(\boldsymbol{r}) &= \int d\boldsymbol{r}\, e^{-i[\alpha\sigma_y(x_j - x_i) - \alpha\sigma_x(y_j - y_i) + B_0x(y_j - y_i)]} w_i^*(\boldsymbol{r})w_j(\boldsymbol{r}) \\ &= e^{-i[\alpha\sigma_y(x_j - x_i) - \alpha\sigma_x(y_j - y_i)]}\int dx\, e^{-iB_0x(y_j - y_i)} w_i^*(x)w_j(x) \\ &\quad\times \int dy\, w_i^*(y)w_j(y).\end{aligned} \tag{14}$$

For integration along the x axis, $y_j - y_i = 0$, the first integral in (14) causes the entire expression to vanish to

0, owing to the orthogonality of the Wannier functions $w_i(x)$, i.e., $\int d\boldsymbol{r} w_i^*(\boldsymbol{r}) w_j(\boldsymbol{r}) = \delta_{ij}$. For integration along the y axis the second integral in (14) makes the total integral 0 because of the orthogonality of the Wannier functions $w_i(y)$. Hence we establish orthonormality, under the nearest-neighbor approximation:

$$\int d\boldsymbol{r} W_i^*(\boldsymbol{r}) W_j(\boldsymbol{r}) = \delta_{ij}. \tag{15}$$

The action of the covariant derivative on this modified Wannier function can be shown to be (recall that $\hat{\boldsymbol{\Pi}} = -i\hbar\boldsymbol{\nabla} + m\boldsymbol{A}$)

$$\hat{\boldsymbol{\Pi}} W_i(\boldsymbol{r}) = e^{-i\frac{m}{\hbar}\int_{r_i}^{r_j} \frac{\hbar}{i} \boldsymbol{A}(\boldsymbol{r}')\cdot d\boldsymbol{l}} \boldsymbol{\nabla} w_i(\boldsymbol{r}). \tag{16}$$

Substituting Eq. (12) in the effective Hamiltonian in (11) and using Eqs. (14) and (16), we obtain

$$\begin{aligned}\hat{H}_A &= \int d^2r \hat{\boldsymbol{\Psi}}^\dagger(\boldsymbol{r}) \frac{\hat{\boldsymbol{\Pi}}^2}{2} \hat{\boldsymbol{\Psi}}(\boldsymbol{r}) = \frac{1}{2}\sum_{i,j} \begin{pmatrix} \hat{b}_{\uparrow i}^\dagger & \hat{b}_{\downarrow i}^\dagger \end{pmatrix} \\ &\times \int d^2r W_i^*(\boldsymbol{r}) \boldsymbol{\Pi}^2 W_j(\boldsymbol{r}) \begin{pmatrix} \hat{b}_{\uparrow j} \\ \hat{b}_{\downarrow j} \end{pmatrix} \\ &= \sum_s \left(\sum_i E_{ii} \hat{b}_{si}^\dagger \hat{b}_{si} + \sum_{\langle i,j\rangle} \hat{b}_{si}^\dagger E_{ij} e^{-i\phi_{ij}} \hat{b}_{sj} \right) = E_0 \hat{\mathcal{N}} + E \hat{\mathcal{T}},\end{aligned} \tag{17}$$

$$\begin{aligned}\hat{H}_I &= \int d^2r \sum_s \hat{\Psi}_s^\dagger(\boldsymbol{r}) \hat{U}_{\rm lat} \hat{\Psi}_s(\boldsymbol{r}) = U_0 \hat{a}^\dagger \hat{a} \sum_{i,j} \begin{pmatrix} b_{\uparrow i}^\dagger & b_{\downarrow i}^\dagger \end{pmatrix} \\ &\times \int d^2r W_i^*(\boldsymbol{r}) [\cos^2(Kx) + \cos^2(Ky)] W_j(\boldsymbol{r}) \begin{pmatrix} \hat{b}_{\uparrow j} \\ \hat{b}_{\downarrow j} \end{pmatrix} \\ &= U_0 \hat{a}^\dagger \hat{a} \sum_s \left(\sum_i J_{ii} \hat{b}_{si}^\dagger \hat{b}_{si} + \sum_{\langle i,j\rangle} \hat{b}_{si}^\dagger J_{ij} e^{-i\phi_{ij}} \hat{b}_{sj} \right) \\ &= \hat{U}_0 \hat{a}^\dagger \hat{a} (J_0 \hat{\mathcal{N}} + J_1 \hat{\mathcal{T}}).\end{aligned} \tag{18}$$

Unlike the case of the BHM in a classical optical lattice [24], for a lattice generated by quantum light we have treated the matrix elements of the potential and kinetic energy separately. This is because of the presence of the term $\hat{a}^\dagger\hat{a}$ in the potential term. So the modified Bose-Hubbard Hamiltonian becomes

$$\begin{aligned}\hat{\mathcal{H}}_{\rm eff}^{(2)} &= E_0 \hat{\mathcal{N}} + E_1 \hat{\mathcal{T}} + \hbar U_0 \hat{a}^\dagger \hat{a} (J_0 \hat{\mathcal{N}} + J_1 \hat{\mathcal{T}}) - \hbar \Delta_c \hat{a}^\dagger \hat{a} \\ &- i\hbar\eta(\hat{a} - \hat{a}^\dagger) + \frac{1}{2}\sum_{i,s,s'} U_{s,s'} b_{is}^\dagger b_{is'}^\dagger b_{is'} b_{is}.\end{aligned} \tag{19}$$

Here E_0 (E_1) and J_0 (J_1) are the on-site (off-site) elements of E_{ij} and J_{ij}, respectively, and these are

$$E_{ij} = \frac{\hbar^2}{2m} \int d^2r w_i^*(\boldsymbol{r}) \boldsymbol{\nabla}^2 w_j(\boldsymbol{r}), \tag{20a}$$

$$J_{ij} = \int d^2r w_i^*(\boldsymbol{r}) [\cos^2(Kx) + \cos^2(Ky)] w_j(\boldsymbol{r}). \tag{20b}$$

$\hat{\mathcal{N}} = \sum_{s,i} \hat{b}_{si}^\dagger \hat{b}_{si}$ is the total atom number operator and $\hat{\mathcal{T}} = \sum_s \sum_{\langle i,j\rangle} \hat{b}_{si}^\dagger e^{-i\phi_{ij}} \hat{b}_{sj}$ is the nearest-neighbor hopping operator; for the full form of $\hat{\mathcal{T}}$ see Appendix B. Here ϕ_{ij} is the phase acquired by an atom while hopping from lattice site i to lattice site j:

$$\phi_{ij} = \alpha\sigma_y(x_j - x_i) + \beta\sigma_x(y_j - y_i) + \mathbb{1}B_0 x_i (y_j - y_i). \tag{21}$$

Here $\mathbb{1}$ is a 2×2 unit matrix. Because of the dynamical nature of the lattice (the coefficient term for the lattice potential involves operators), E_{ij} and J_{ij} are treated separately; otherwise the hopping amplitude would be identified with $t = E_1 + J_1$ and the chemical potential with $\mu = E_0 + J_0$.

III. ELIMINATION OF CAVITY DEGREES OF FREEDOM

A. The effective model

The interplay of energy scales associated with the spin-orbit coupling, motion of atoms in a dynamical lattice, and atom-atom interactions brings out a richer and more complex dynamics compared to the usual BHM [16,24], which we try to capture through the light coming out of the cavity. To facilitate further discussion on dynamics governed by (19) we do certain simplifications based on the typical experimental systems. Following the typical experimental situation [12–14] we work under a bad cavity limit, where we assume that the cavity field reaches its stationary state much more quickly than the time scale involved with atomic dynamics. Hence it is reasonable (at least for $t > 1/\kappa$) to replace the light field operators with their steady-state values and, thus, adiabatically eliminate the cavity degrees of freedom from the Hamiltonian, (19), so that it depends only on the atomic variables. It will be useful to remember that this process is distinct from the adiabatic elimination of excited state $|1\rangle$, reported in the previous section. The evolution of light field operators can be obtained from (19) as

$$\partial_t \hat{a} = \frac{1}{i\hbar}[\hat{a}, \hat{H}_{\rm eff}^{(2)}] = -\hat{D}\hat{a} + \eta, \tag{22}$$

where $\hat{D} = \kappa + i[U_0(J_0\hat{\mathcal{N}} + J_1\hat{\mathcal{T}}) - \Delta_c]$ is a complex operator. Assuming the total number of atoms to be fixed, we can replace the atom number operator by a fixed quantity, $N_0 = \langle\hat{\mathcal{N}}\rangle$, and due to the presence of atoms an effective detuning is obtained as $\Delta_c' = \Delta_c - U_0 J_0 N_0$. Setting $\partial_t \hat{a} = 0$ we get the steady-state value $\hat{a}^{(s)} = \eta/\hat{D}$ and then expand $\hat{a}$ with respect to the hopping matrix $\hat{\mathcal{T}}$:

$$\hat{a}^{(s)} \approx \frac{\eta}{\kappa - i\Delta_c'} \left[1 - \frac{iU_0 J_1}{\kappa - i\Delta_c'} \hat{\mathcal{T}} - \frac{U_0^2 J_1^2}{(\kappa - i\Delta_c')^2} \hat{\mathcal{T}}^2 + \cdots \right]. \tag{23}$$

Substituting this in the Hamiltonian, (19), we obtain the effective Hamiltonian, expressed in terms of atomic variables:

$$\hat{\mathcal{H}}_{\rm eff}^{(3)} = -\tilde{J}_0 \hat{\mathcal{T}} + \tilde{J}_1 \hat{\mathcal{T}}^2 + \cdots + \frac{1}{2}\sum_{i,s,s'} U_{s,s'} \hat{b}_{is}^\dagger \hat{b}_{is'}^\dagger \hat{b}_{is'} \hat{b}_{is}, \tag{24}$$

$$\tilde{J}_0/J_1 = U_0\eta^2 \frac{\kappa^2 - \Delta_c'^2}{\left(\kappa^2 + \Delta_c'^2\right)^2} - E/J_1, \tag{25a}$$

$$\tilde{J}_1/J_1^2 = 3U_0^2\eta^2\Delta_c' \frac{3\kappa^2 - \Delta_c'^2}{\left(\kappa^2 + \Delta_c'^2\right)^4}. \tag{25b}$$

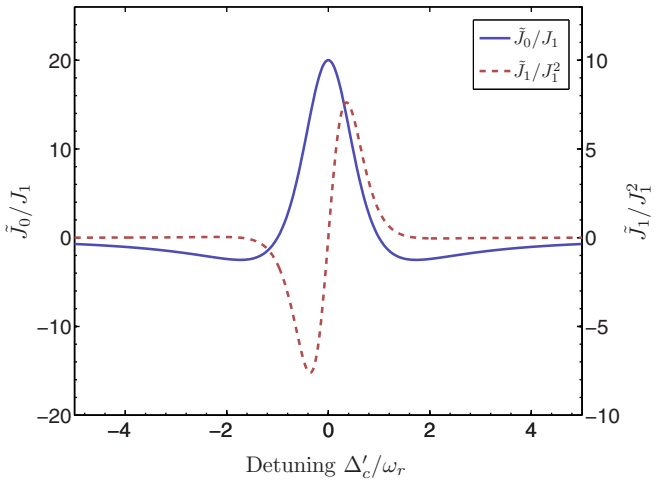

FIG. 2. (Color online) Variation of the two coefficients used in (24) with effective detuning. Experimental parameters are set to be $\{\eta,\kappa,U_0,J_0\} = \{10,1,0.2,2\}\omega_r$.

The parameter $\tilde{J}_0$ is the rescaled hopping amplitude, where the scaling factor is introduced by the cavity parameters and that of the atom-photon interaction strength. Its variation with cavity detuning is shown in Fig. 2. Note that $\tilde{J}_0$ can be made to vanish by setting $\Delta_c' = \kappa$, and similarly, $\tilde{J}_1$ vanishes when $\Delta_c' = \sqrt{3}\kappa$.

It is clear from (24) that cavity-atom coupling induces higher order hoppings feasible through terms like $\hat{\mathcal{T}}^{(n)}$. Also, the amplitude of these terms are well controllable through cavity parameters, allowing us to study higher order atom-atom correlations in these systems. Through suitable choice of cavity parameters, we suppress all higher order terms starting from $\hat{\mathcal{T}}^2$. This renders $\hat{\mathcal{H}}^{(3)}_{\rm eff}$ to a tight-binding Hamiltonian [41], which incorporates the effects of cavity, Abelian gauge field, and non-Abelian gauge field altogether:

$$\hat{\mathcal{H}}^{(4)}_{\rm eff} = -\tilde{J}_0\hat{\mathcal{T}} + \frac{1}{2}\sum_{i,s,s'} U_{s,s'}\hat{b}^\dagger_{is}\hat{b}^\dagger_{is'}\hat{b}_{is'}\hat{b}_{is}. \tag{26}$$

This is our effective Bose-Hubbard Hamiltonian, on which the rest of the work is built. The hopping amplitude is $\tilde{J}_0$. The hopping operator $\hat{\mathcal{T}}$ now contains all the information about spin-orbit coupling. However, it may be pointed out that, apart from the modifying bare hopping amplitude J_0 to the rescaled $\tilde{J}_0$, the cavity also triggers long-range correlations via higher order terms in $\hat{\mathcal{T}}$ which we ignored. In fact in the presence of a dynamical lattice both the atom and the photon operators evolve, in accordance with their corresponding (coupled) Heisenberg equations [38]. One can solve this pair of equations simultaneously to study the full self-organization. However, assuming that the atoms fall through the cavity light field sufficiently faster (much before the atoms affect the cavity photon), we ignore the backaction of the atoms on the cavity light [40]. Self-organization of atoms in the lattice [19,20] can in itself be a separate direction to pursue, facilitating study of the self-organized checkerboard phase [42], supersolid phase [43], or quantum spin-glass phase [44].

In the following subsection we analyze the complete energy spectrum in the noninteracting limit of the effective Hamiltonian in (26). For this subsection only, we switch off the interatomic interaction, namely, $U_{s,s'} = 0$, which can be achieved by tuning the s-wave scattering length a_s to 0 using the Feshbach resonance method [45]. For ^{85}Rb this can be achieved at a low magnetic field and for various scattering channels [46]. However, in recent times there also has been a lot of progress in tuning the scattering length of ^{87}Rb, whose hyperfine states we consider in our work. Feshbach resonances in ^{87}Rb were first identified via magnetic tuning in [47], and later many alternative ways were also developed, such as light-induced resonances [48] and via stimulated Raman coupling [49].

B. The spectrum: Noninteracting limit

Rescaling of the hopping amplitude by the cavity parameters allows a number of physical properties to be controlled through such parameters. We study the spectrum of this tight-binding Hamiltonian obtained in (26). We reiterate that the analysis in this section is in the absence of an atom-atom interaction. We show that the resulting system yields two interesting spectra, namely, the Hofstadter butterfly spectrum [50] and the Dirac spectrum. The emergence of the Hofstadter spectrum is natural, as the considered noninteracting bosonic system mimics the motion of a Bloch particle (a quantum mechanical particle in a periodic lattice potential) in the presence of a uniform U(1) gauge field. The energy levels of such a particle is the Hofstadter spectrum: a butterfly-like structure is revealed when the energy value of the Bloch particle is plotted against the Abelian flux inserted. Such is the case in the absence of spin-orbit coupling ($\alpha = 0$), where the Hamiltonian in (26) becomes identical to a Harper Hamiltonian, which can be obtained through Peierl's substitution in the usual tight-binding Hamiltonian [50]. Recently, two groups, at MIT and in Munich, have experimentally realized such a butterfly spectrum in cold atomic systems [51]. However, compared to those systems, in the present case one can control (through suitable choice of $\tilde{J}_0$) the energy scale of the butterfly structure just by suitably tuning the cavity parameters. The effects of a non-Abelian gauge field on such a butterfly structure have also been studied [52].

Next we show how the Dirac spectrum emerges. For this the Hamiltonian in (26) is diagonalized in Appendix B 1, and the spectrum obtained is

$$E_\pm/\tilde{J}_0 = 2\cos\alpha\cos k_x + 2\cos\beta\cos(k_y - 2m\pi\Phi) \pm \sqrt{\sin^2\alpha\sin^2 k_x + \sin^2\beta\sin^2(k_y - 2m\pi\Phi)}, \tag{27}$$

where (m,n) is a lattice point. The energy values are plotted against the particle momentum and a Dirac-like spectrum is obtained as shown in Fig. 3.

The band splitting in the spectrum becomes evident as soon as the effects of SOC are incorporated, showing a band gap (E_g) of $E_g/\tilde{J}_0 = 4\sin\alpha\sqrt{\sin^2 k_x + \sin^2(k_y - 2m\pi\Phi)}$, where the gap can be tuned by the cavity as well (through $\tilde{J}_0$). Also, in the first Brillouin zone the band gap is maximum when $(k_x,k_y) \in \{(\pm\pi/2, \pm\pi/2)\}$ and $E_g^{\rm max}/\tilde{J}_0 = 4\sqrt{2}\sin\alpha \equiv W$. It is possible to carry out a band-gap measurement in such systems via Bragg spectroscopy [53], through which one can measure the non-Abelian flux inserted in the system. However, the gap vanishes when both $\sin k_y = \sin k_x = 0$.

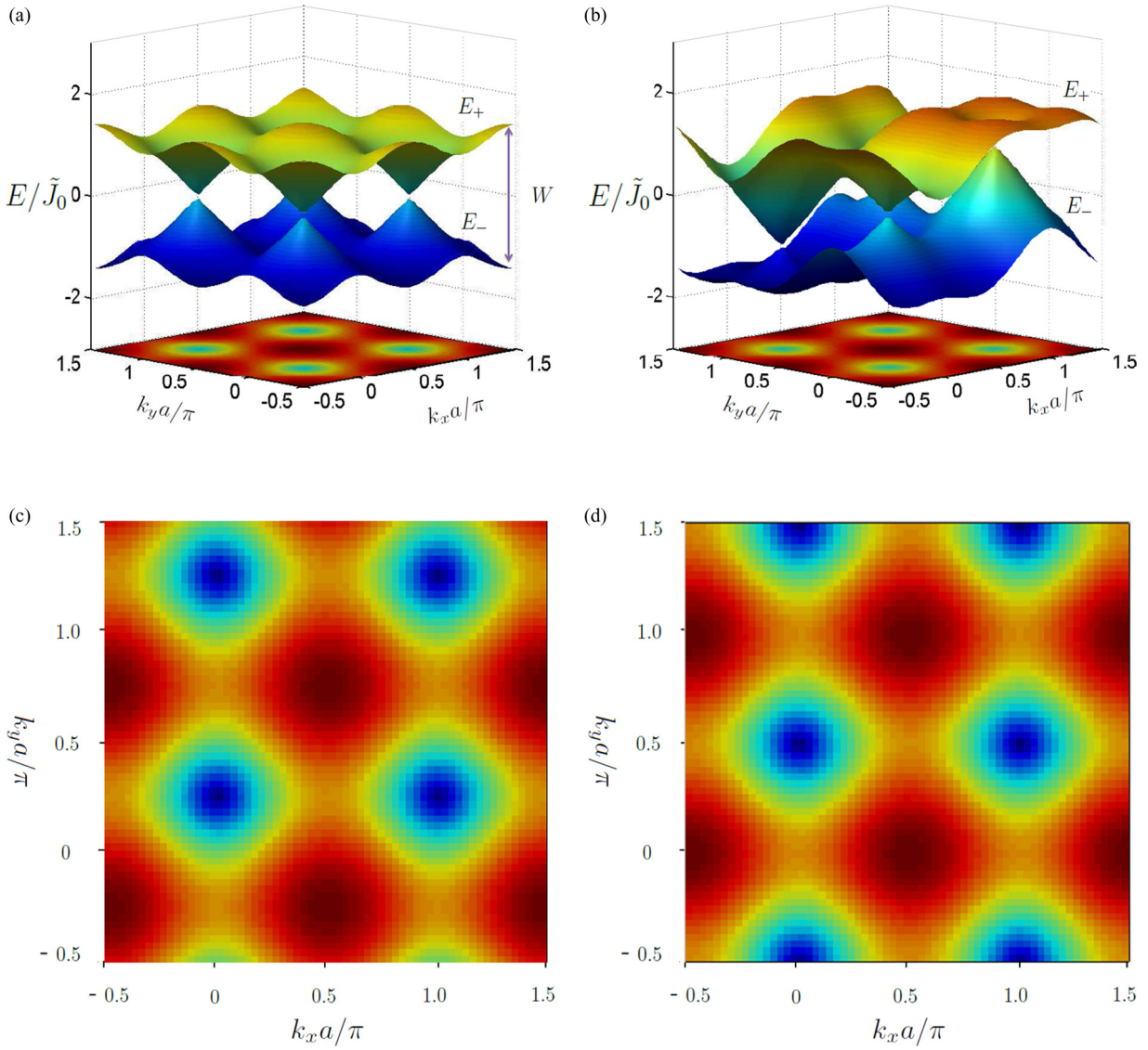

FIG. 3. (Color online) Three-dimensional view of the energy spectrum plotted for a purely ($\Phi = 0$ non-Abelian gauge field. The strength of SOC is (a) $\alpha = \pi/2 = \beta$ and (b) $\alpha = \pi/2 + 0.25$, $\beta = \pi/2 - 0.25$. The surface plot is an intensity map of the energy difference between E_+ and E_-. The four green spots on the surface correspond to the four (bosonic) Dirac points (at the zone centers) where the energy gap between the two bands vanishes. The red band and blue band correspond to E_+ and E_-, respectively. W is the maximum band gap, which occurs at the zone boundaries. (c, d) Location of the Dirac points on the momentum space are shown for $2m\pi\Phi = 0.75$ and 1.5, respectively. With increasing Φ the Dirac points move along the positive k_y axis.

In the first Brillouin zone (by setting $\Phi = 0$) this can happen for $(k_x,k_y) \in \{(0,0),(\pm\pi,0),(0,\pm\pi),(\pm\pi,\pm\pi)\} \equiv \boldsymbol{k}_D$. In the vicinity of these points the effective low-energy behavior can be described (see Appendix B 1 for details) by a Dirac-like Hamiltonian:

$$\hat{H}_{\text{eff}} = -\sum_{\boldsymbol{p}} \hat{\Psi}^\dagger_{\boldsymbol{p}} \hat{H}_D \hat{\Psi}_{\boldsymbol{p}}, \quad \hat{H}_D = c_x \gamma_x p_x + c_y \gamma_y p_y. \quad (28)$$

Here $\hat{H}_D$ is a Dirac Hamiltonian, $\boldsymbol{p} = \boldsymbol{k} - \boldsymbol{k}_D$, but the field operators $\hat{\Psi}_{\boldsymbol{p}}$ are bosonic annihilation operators. The γ matrices $\gamma_0 = \mathbf{1}$, $\gamma_1 = \gamma_x = \sigma_y$, and $\gamma_2 = \gamma_y = \sigma_x$ are the $(2+1)$-dimension representation of Clifford algebra, $\{\gamma_i,\gamma_j\} = 2\delta_{ij}$. The speeds of light $c_x = 2\sin\alpha$ and $c_y = 2\sin\beta$ are now anisotropic. As shown in Fig. 3, through this anisotropy the SOC strength can be used as a handle for controlling the shape of the Dirac cones. We refer to the "Dirac-like" points $\boldsymbol{k}_D$ in our bosonic system also as Dirac points. Near $\boldsymbol{k}_D$ the excitation quasiparticles are massless bosons having a dispersion relation linear in $\boldsymbol{k}$, the slope of which is controlled by adjusting the spin-orbit coupling strength.

It must be emphasized that such massless bosonic quasiparticles which mimic massless dirac fermions in relevant fermionic systems [53] arise in this system as a consequence of the spin-1/2 nature of the bosons. Such spin-1/2 bosons have no natural analog because of Pauli's spin-statistics theorem. However, this constraint can be lifted by synthetic symmetries [54] and a synthetic bosonic (pseudo-) spin-1/2 system can be realized [10]. Soon after the preliminary proposals on simulation of Dirac fermions in cold-atom systems [55] they

were realized experimentally [53], using density profile measurement methods or Bragg spectroscopy. Similar techniques may also be exploited to observe the bosonic quasiparticles that follow the massless Dirac equation.

As is evident from Eq. (27), the effect of an Abelian field would be to move these points in the momentum space [see Figs. 3(c) and 3(d)]. With a finite Abelian field there also emerges a Hofstadter spectrum as discussed previously. This can be verified by plotting the energy as a function of the Abelian (magnetic) flux [52]. For the same system in Figs. 3(c) and 3(d) we plot the energy versus the Bloch momentum for a given value of the Abelian flux to show the location of the Dirac points. By Eq. (27) it is also suggested that, with the use of a spatially modulated Abelian flux, one may control the separation between the Dirac points. Motion and merging of Dirac points are also very interesting, as they lead to topological phase transitions [56]. One can also switch on the interaction and study its effects on the spectrum [57].

C. Emerging magnetic orders

In this subsection we discuss the various magnetic orders that arise in the ground state of the Hamiltonian, Eq. (26). This can be done by mapping this Hamiltonian to an effective spin Hamiltonian: one treats the interaction part of Eq. (26) as the zeroth-order Hamiltonian and then the hopping part ($\tilde{J}_0\hat{\mathcal{T}}$) is treated perturbatively to get the effective spin Hamiltonian matrix elements. We do not discuss the full method here; this can be found in [9] and [58–60]. Using such an analysis the effective spin Hamiltonian of an SOC BEC in a classical optical lattice was obtained in [26–29]. We realize that the mathematical structure of our effective mBHM Hamiltonian, Eq. (26), is the same as that considered in [26–29], provided we switch off the Abelian-field part. Since we have considered a cavity-induced quantum optical lattice, instead of the hopping amplitude t in a classical optical lattice, which was the case studied in those works, here we have a rescaled hopping parameter $\tilde{J}_0$, which essentially captures the information on the quantum light. Thus in the parent Hamiltonian in Refs. [26–29], if we substitute $\tilde{J}_0$ in place of t, we arrive at the same conclusion. In fact, since $\tilde{J}_0$ can be controlled by means of the cavity parameters, one can also maneuver the entire phase diagram by suitably adjusting these parameters.

Thus we consider the spin Hamiltonian obtained in [28] and directly substitute $\tilde{J}_0$ in place of t to obtain

$$\begin{aligned}
\hat{H}_{\rm spin} &= \hat{H}_H + \hat{H}_A + \hat{H}_D,\\
\hat{H}_H &= -\sum_i \mathcal{H}\vec{S}_i\cdot(\vec{S}_{i+\delta_x}+\vec{S}_{i+\delta_y}),\\
\hat{H}_A &= -\sum_i \mathcal{A}\big(S_i^x S_{i+\delta_x}^x + S_i^y S_{i+\delta_y}^y\big),\\
\hat{H}_D &= -\sum_i \mathcal{D}\big(\vec{S}_i\times\vec{S}_{i+\delta_x}\cdot\hat{x}+\vec{S}_i\times\vec{S}_{i+\delta_y}\cdot\hat{y}\big),
\end{aligned}\tag{29}$$

Here $\vec{S}_i$ are the isospin operators at site i: $\vec{S}_i=\frac{1}{2}\sum_{s,s'}\hat{b}_{si}^\dagger\vec{\sigma}_{ss'}\hat{b}_{s'i}$. The components of the isospin operator are $S_i^x=(\hat{b}_{\uparrow,i}^\dagger\hat{b}_{\downarrow,i}+\hat{b}_{\downarrow,i}^\dagger\hat{b}_{\uparrow,i})/2$, $S_i^y=(\hat{b}_{\uparrow,i}^\dagger\hat{b}_{\downarrow,i}-\hat{b}_{\downarrow,i}^\dagger\hat{b}_{\uparrow,i})/2i$, and $S_i^z=(\hat{b}_{\uparrow,i}^\dagger\hat{b}_{\uparrow,i}-\hat{b}_{\downarrow,i}^\dagger\hat{b}_{\downarrow,i})$. And $\mathcal{H}=\frac{4\tilde{J}_0^2}{U}\cos(2\alpha)$, $\mathcal{A}=\frac{8\tilde{J}_0^2}{U}\sin^2\alpha$, and $\mathcal{D}=\frac{4\tilde{J}_0^2}{U}\sin(2\alpha)$ are the spin interaction strengths. The effective spin Hamiltonian $\hat{H}_{\rm spin}$ is a combination of 2D Heisenberg exchange interactions ($\hat{H}_H$), anisotropy interactions ($\hat{H}_A$), and Dzyaloshinskii-Moriya interactions ($\hat{H}_D$) [61]. These terms collectively stabilize the following orders [28]: Ising ferromagnets (zFM), antiferromagnets (zAFM), stripe phase, spiral phase (commensurate with three-site or four-site periodicity, denoted, respectively, 3-spiral and 4-spiral), and vortex (VX) phase.

A detailed discussion of these phases can be found in [28]. We discuss them briefly. Schematics of the spin configurations of these phases are given in the insets in Fig. 5. The zFM order is a uniformly ordered phase where all the spins are aligned along the z axis, however, in the zAFM phase the direction of the spin vectors alternates between parallel and antiparallel to the z axis. There is a subtle difference between the stripe phase and the zAFM: in the stripe phase, along a given axis on the xy plane all spins are up, but for the other axis they alternate between up and down. In the zAFM phase the spins alternate along both axes. Two types of spiral waves appear in this system. In both cases, all the spins along one axis on the xy plane are parallel, however, along the other axis, the spin vectors make an angle with the z axis which changes (starting from 0) as we move along the axis. However, there exists a period in the number of lattice sites after which the angles are repeated like waves. In 4-spirals, four sites make one period: the angles progress with the site as π, $\pi/2$, 0, $-\pi/2$,π, ... In 3-spirals, three sites make one period: the angles progress with the site as π, $\pi/3$, $-\pi/3$, π, ... The VX phase is one of the xy phases, in which all the spin vectors lie on the xy plane. In Sec. IV we see how we can detect all these phases.

IV. THE CAVITY SPECTRUM FOR THE MAGNETIC PHASES

In the preceding section, we discuss the spectrum of noninteracting SOC bosons in a cavity-induced quantum optical lattice potential. Now we switch on the atom-atom interaction. As pointed out in Sec. III C this causes the appearance of various magnetic orders in the many-body quantum mechanical ground state. These orders have been studied in cold atomic systems, in the presence [26–29] or absence [58–60] of SOC. The many-body wave function has an orbital part and a spinorial part, and the magnetic orders are characterized by the spinorial part of the wave function. Detection of various phases in the orbital part of the wave function, through the cavity spectrum, was carried out in [16]. In our work we propose a method which enables us to probe the spinorial part of the wave function (hence the magnetic orders) with the help of the cavity spectrum.

We define the cavity spectrum as the steady-state outcoming (leakage) photon number, which is obtained from (22) by setting $\partial_t\hat{a}=0$ as

$$n_{\rm ph}=\langle\hat{a}^{\dagger(s)}\hat{a}^{(s)}\rangle_\Psi=\frac{\eta^2}{\kappa^2+(\Delta_c'-U_0J_1\langle\hat{\mathcal{T}}\rangle_\Psi)^2}.\tag{30}$$

The corresponding expression in the laboratory frame and its relation to this expression are discussed in Appendix A 2. This equation is nonlinear [62] in terms of the photon density

$n_{\rm ph}$ since the tunneling parameters J_0 and J_1 are dependent on the depth of the optical lattice potential, $V_0 = U_0 n_{\rm ph}$. Essentially, the cavity induces a feedback mechanism (of cavity light) causing the cavity spectrum to nonlinearly depend on $n_{\rm ph}$ through this modified Lorentzian [63]. In addition, the spectrum is also dependent on the state $|\Psi\rangle$ through the expectation value of the hopping operator $\langle\hat{T}\rangle_\Psi$. This dependence is pronounced only when J_1 is finite. In further discussion we show how this dependence can be used to probe the spinorial part of the quantum many-body ground-state wave function.

The ground state of the BHM is controlled by the value of t/U [26,64]. As the depth of the potential well increases, the ground state changes from an SF to an MI state. To simplify our discussion we assume that the orbital (optical lattice site) part of the wave function corresponds to an MI state with one atom per lattice site. In the absence of any (synthetic) gauge field, for a 2D lattice, this phase boundary occurs at $U = 4(3+2\sqrt{2})t$, which can be obtained from mean-field calculations [65]. The presence of a (synthetic) Abelian gauge field further localizes the atoms and the phase boundary gets shifted towards a larger value of t/U or a more shallow lattice [66]. So we confine our discussion to lattice depths larger than $20E_r$.

We further divide the MI regime into two regions separated at a potential depth of $25E_r$ [see Fig. 4(a)]. In one region of the depth values J_1 vanishes, hence it becomes impossible to probe the spinorial part of the ground state through the cavity spectrum. In the other region J_1 is finite, enabling us to probe the ground state. We term these regions as follows: region I—the shallow MI regime ($\lesssim 25E_r$), where $J_1 \neq 0$ and hence Eq. (30) is highly nonlinear; and region II—the deep MI regime ($\gtrsim 25E_r$), where J_1 is approximated as 0 and the nonlinearity in $n_{\rm ph}$ enters only through J_0.

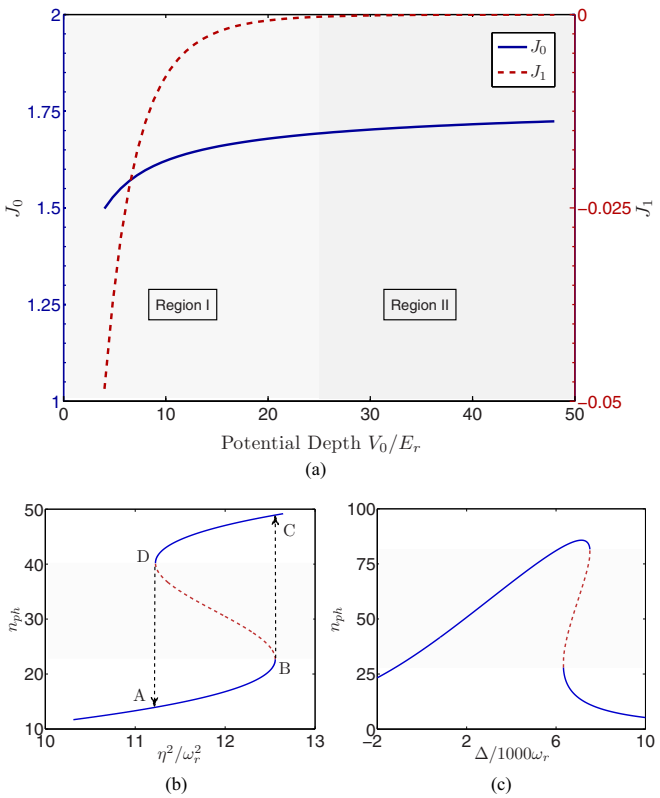

FIG. 4. (Color online) (a) Variation of overlap integral elements with potential depth. We study the variation in two regions, separated at $V = 25E_r$: cavity spectrum for a deep lattice (region I) and for a 6×6 lattice, $\{U_0,\kappa\} = \{12,1\}\omega_r$. (b) Variation with pump amplitude η for $\Delta_c = 5000\omega_r$. (c) Variation with detuning Δ_c for $\eta = 6\omega_r$. Dotted (red) lines are unstable regions of the photon count.

Let us first consider region II. As shown in Figure 4(a), in this region J_0 vs V_0 can be approximated by a linear function ($J_0 = aV_0 + b$) and J_1 can be assumed to be 0. The variation of $n_{\rm ph}$ with respect to the pump amplitude η^2 is shown in Fig. 4(b), and that with respect to the detuning Δ_c' is shown in Fig. 4(c). There exists a bistable region in the spectrum, which is shown by the dashed (red) line. In the strong MI regime the atoms get tightly localized at their site, resulting in a negligible hopping amplitude. The atoms can sense the presence of the Abelian or non-Abelian field only through the hopping term, and now since the hopping amplitude is almost negligible, the cavity spectrum is insensitive to the Abelian or non-Abelian gauge field.

As the pumping amplitude η decreases the photon number decreases [see Fig. 4(b)], however, at a certain point (point D) the photon number abruptly drops to a very small value (point A), hence the lattice suddenly becomes very shallow. This causes a phase transition from the MI to the SF phase. Similarly, as η increases the photon number also increases, as does the lattice depth. At point B it suddenly jumps to a large value of $n_{\rm ph}$ (point C), hence a phase transition from SF to MI occurs. This is an instance of a bistability-driven phase transition, which was previously pointed out in [22] and [62], in different contexts. Points B and D are often referred to as turning points or critical points. When the photon number decreases one might end up in the SF phase or one might stay in the shallow MI region. So to determine the phase exactly one needs to obtain the exact phase diagram and locate the appropriate turning points. We do not extend this discussion further.

Now we turn to the case of the shallow MI regime (or region I). We separate the following section, where we show that in this region it is feasible to probe the ground state of an SOC BEC through the cavity spectrum. When $J_1 \neq 0$, the Lorentzian, (30), can sense the presence of the magnetic orders through $\langle\hat{T}\rangle$. In Sec. III C we have introduced and briefly discussed the magnetic order that prevails in such a system.

Before getting to our results, it is worthwhile pointing out that after the realization of spin-orbit coupling for bosonic clouds [10] or condensates [4] by Spielman's group, the phase diagram of such a system was theoretically obtained by various groups in [26–29]. Experimental verification of these phases might not be very trivial; most importantly, detecting all the emergent phases using a single experimental setup is a formidable task. So far, the method of spin structure factor measurement through Bragg spectroscopy [67] has been commonly used. Other methods include measurement of spatial noise correlations [68], polarization-dependent phase-contrast imaging [69], and direct imaging of individual lattice sites [70]. However, each of these techniques comes with its own set of complications.

Extending the idea which was originally espoused for BECs without spin degrees of freedom [16] here we propose a

different scheme of experiments where such magnetic orders can be ascertained without making a direct measurement on the atomic system. The relation between this approach and the "quantum nondemolition measurement" technique has also been discussed [17,20,43]. The method facilitates the detection of all possible phases arising in the Mott regime of an SOC BEC, and this can also be extended to the SF regime.

With this purpose we work out the values of $\langle\hat{\mathcal{T}}\rangle$ and obtain the cavity spectrum. Following [71] the wave function for various orders can (in the Mott phase only) be written as

$$|\Psi_{\mathrm{MI}}\rangle = \prod_{i\in A, j\in B} |\psi_A\rangle_i |\psi_B\rangle_j, \tag{31}$$

with site indices i and j and $|\psi_{A,B}\rangle = \cos\frac{\theta_{A,B}}{2}|\uparrow\rangle + e^{i\phi_{A,B}} \sin\frac{\theta_{A,B}}{2}|\downarrow\rangle$. The entire lattice is divided into two sublattices, A and B, and we assume that alternating sites belong to different sublattices. The parameters θ and ϕ are projection angles in the internal spin space. We assume that there are exactly equal numbers of lattice sites in sublattices A and B, hence the total number of sites is K^2 even; also, assuming unit filling we set $K^2 = N_0$. Please note that K was used earlier to denote the wave number of the cavity photon and here we use the same notation for a different thing. In Appendix B 2 we calculate the expectation value of the tunneling operator $\langle\hat{\mathcal{T}}\rangle$ for various magnetic orders and summarize them in Table I. This is the basis of further discussions. We can distinguish between different magnetic orders because each order can now be associated with a corresponding $\langle\hat{\mathcal{T}}\rangle$, hence a cavity spectrum, *provided* there is a nonvanishing z-axis component of the spin vector (the reason will become clear later). Thus one cannot distinguish between any of the xy phases, such as the VX phase and the anti-VX phase. However, the other various magnetic orders which can arise in an SOC system through experimental control of the free parameters (α,β) [28] or (α,λ) [26,29] can be well distinguished.

TABLE I. Expectations for the hopping operator and the steady-state photon number for different phases in the MI state.

Order	$\hat{\mathcal{T}}$
zAFM	0
Stripe	$2K(K-1)\cos\beta$
VX	$K(K-1)(\cos\alpha+\cos\beta)$
3-spiral	$3K(K-1)(\cos\alpha+4\cos\beta)/8$
4-spiral	$K(K-1)(\cos\alpha+3\cos\beta)/2$
zFM	$2K(K-1)(\cos\alpha+\cos\beta)$

The cavity spectra for each of these orders are shown in Fig. 5. The spin-orbit coupling strength (α,β) for a particular order is chosen such that that specific order gets stabilized

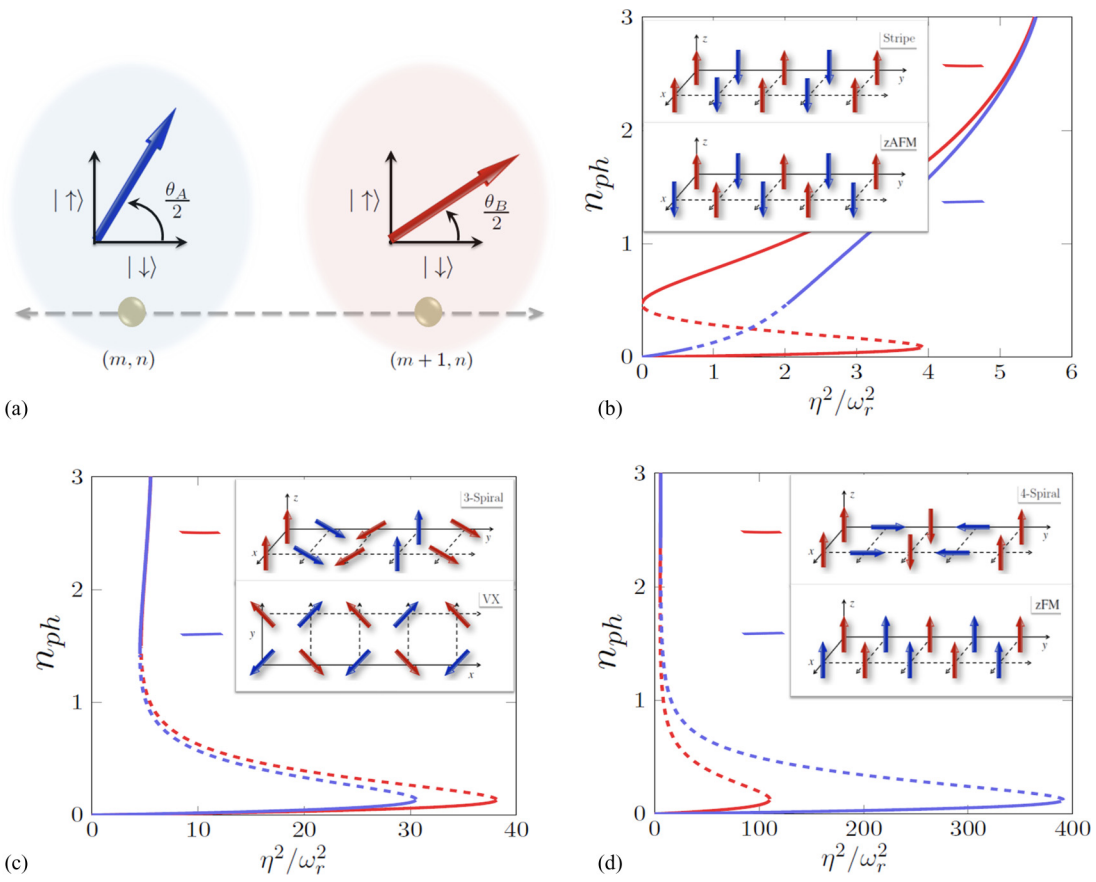

FIG. 5. (Color online) (a) Spin vectors in internal spin spaces of two neighboring sites. (b–d) Cavity spectrum for different phases in the MI region for different non-Abelian flux insertions. The SOC strength for all phases is $(\alpha,\beta)/\pi = (0.01,0.01)$ zFM, (0.2, 0.2) 4-spiral, (0.3,0.3) 3-spiral, (0.5,0.5) stripe, and (0.34, 0.34) VX. Note that the turning points are highly dependent on the phases. The dotted parts of curves show the unstable region of the spectrum. Red and blue legends correspond to the magnetic order, shown in insets.

[28]. As we gradually increase the pump value the photon number gets increased, but at the turning point (η_c) it suddenly jumps to a higher value of photon number, since the photon intermediate count corresponds to the unstable region. Clearly, the behaviors of the spectra for different orders are different; specifically, the value of η_c varies widely. The zAFM will not show any such jump, and the stripe phase will have a very small value of η_c. For the zFM phase η_c will always be the largest and for the 4-spiral phase it would be quite comparable with the η_c of the zFM phase. The xy and 3-spiral phases always have η_c values between these two extremes.

The above discussion is supported by the following observation. In Fig. 5(a) the internal spin (by "spin" we actually refer to "pseudospin") spaces of two neighboring sites are shown as red or blue ovals. The basis vectors of the spin spaces are the eigenvectors of $\hat{S}_z$. If a spin vector makes an angle θ with the z axis in real space, then in the spin space it makes an angle $\theta/2$ with the $\downarrow$ axis. A particular magnetic order is nothing but a specific spatial distribution of these θ and ϕ values. The value of $\langle\hat{\mathcal{T}}\rangle$ is a measure of the probability of spin-dependent hopping across neighboring sites, which hence captures this variation of θ values over the configuration space. We proceed in the following way (see Appendix B 2 for the rigorous derivation): if a spin vector creates an angle θ_A with the z axis and the spin vector at the site nearest to it makes an angle θ_B, then in their internal spin spaces they make an angle $\theta_A/2$ and $\theta_B/2$ with $\downarrow$. Hence the projections of the spin vectors on the $\downarrow$ axis are $\cos\theta_{A,B}/2$ and those on the $\uparrow$ axis are $\sin\theta_{A,B}/2$. The probability of hopping of $\uparrow$ to $\uparrow$ (or $\downarrow$ to $\downarrow$) is the modulus-squared product of the projection lengths along the $\uparrow$ ($\downarrow$) axes. Hence hopping of $\uparrow$ to $\uparrow$ has a probability of $(\sin\frac{\theta_A}{2}\sin\frac{\theta_B}{2})^2$, and for hopping of $\downarrow$ to $\downarrow$ it is $(\cos\frac{\theta_A}{2}\cos\frac{\theta_B}{2})^2$. Since $\uparrow$ and $\downarrow$ are orthogonal vectors, hopping associated with a spin flip is found to have vanishing $\langle\hat{\mathcal{T}}\rangle$.

To illustrate the implication of the above technique consider the case of the zAFM phase. In this phase, at alternative sites

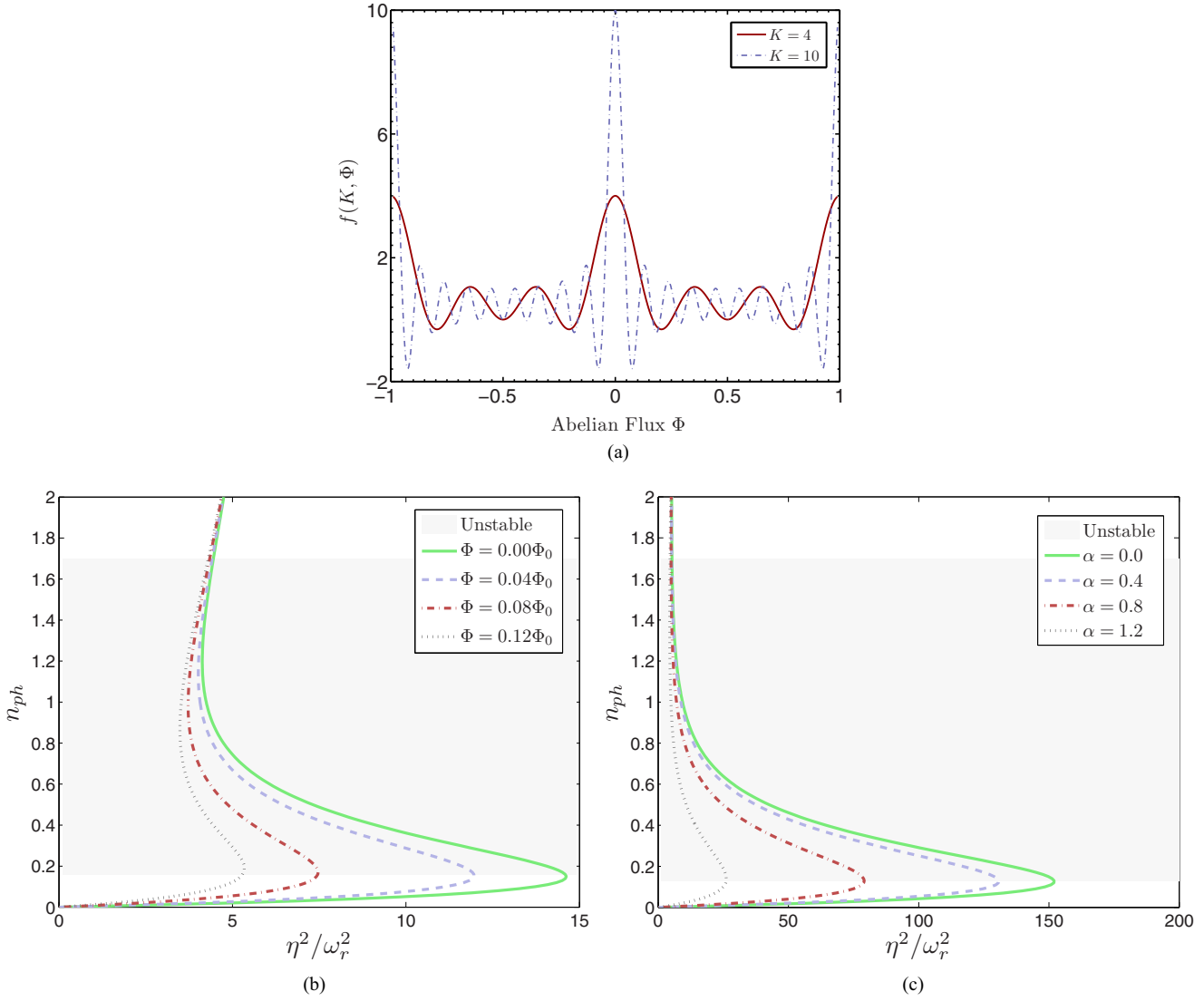

FIG. 6. (Color online) (a) Variation of the grating function $f(K,\Phi)$ with the inserted Abelian flux. Legends indicate the size of the lattice. In a large lattice limit the grating function does not sense the variation of Φ. (b, c) Cavity spectrum for different (b) Abelian fields (with a fixed non-Abelian field, $\alpha = -\beta = \pi/2 - 0.15$) and (c) non-Abelian fields (with a fixed Abelian field, $\Phi = 0.08\Phi_0$). The negative-slope region is the unstable [shaded (gray)] part of the spectrum.

spin vectors are oriented parallel or antiparallel to the z axis, i.e., $\theta_A = 0$, $\theta_B = \pi$. Hence any reordering of the spin vectors (mediated by the cavity light) which does not alter the magnetic order should consist of hopping from $\uparrow$ to $\downarrow$, or vice versa. However, the matrix element $\langle\hat{T}\rangle$ for such hopping is 0. Hence $\langle\hat{T}\rangle_{\text{zAFM}} = 0$ (see Table I). Similarly in the case of zFM all spin vectors are aligned along the z axis, i.e., $\theta_A = \pi = \theta_B$. Hence any hopping other than $\uparrow$ to $\uparrow$ will have a vanishing contribution in $\langle\hat{T}\rangle_{\text{zFM}}$ and $\langle\hat{T}\rangle_{\text{zFM}} \propto (\sin\pi/2 \sin\pi/2)^2$. It must be noted that the value of $\langle\hat{T}\rangle$ in turn controls the value of η_c, hence the trend of variation in $\langle\hat{T}\rangle$ with respect to the phases gets mapped to that in the values of η_c. The $\cos\alpha$ and $\cos\beta$ are just scaling factors introduced because of spin-orbit coupling. This is the central result of our work. Now we show that, other than the phase information, the cavity spectrum can also be used to extract the amount of Abelian or non-Abelian flux inserted in the system.

In order to show how the cavity spectra can be used for flux detection we consider the zFM phase, which is stabilized in the presence of both an Abelian and a non-Abelian field [66]. In the presence of an Abelian flux, the expectation value for the tunneling operator for zFM order becomes (see Appendix B 2) $\langle\hat{T}\rangle_{\text{FM}} = 2\cos\alpha(K-1)[K + f(K,\Phi)]$. The presence of the Abelian flux gives additional phases to the hopping, thus resulting in an overall phase factor of $f(K,\Phi) = \frac{\sin(K\pi\Phi)}{\sin(\pi\Phi)}\cos[\pi\Phi(K-1)]$. This function is plotted in Fig. 6(a). The similarity of the functional form of $f(K,\Phi)$ with that of an N-slit grating function is just because in this case the phases arising due to the presence of this field get summed over to yield such a function. Evidently the optical lattice acts as a quantum diffraction grating [16,72].

V. CONCLUSION

To summarize, in this paper we have derived an effective model, i.e., Eq. (26), for an SOC BEC inside a cavity. The subsequent analysis based on this effective model indicates a number of very interesting features. We first studied its spectrum in the noninteracting limit and showed that a Dirac-like spectrum arises for such ultracold bosons because of the effective spin-1/2 behavior of this system. We also point out that in the presence of Abelian flux, one can generate a highly controllable (through cavity parameters) Hofstadter butterfly spectrum.

Then we discuss the magnetic phases that arise in the MI-type ground state of this Hamiltonian after including atom-atom interaction. Subsequently we discuss a technique with which we can probe these magnetic orders through the cavity spectrum. By setting up a lattice, generated by the cavity, we first let the atoms stabilize in a particular magnetic order. This can be done by adjusting the spin-orbit coupling strengths α and β and the interatomic interaction strengths $U_{s,s'}$. Then we count the photons leaking out of the cavity as we increase the pump-laser amplitude (η). We observe at a certain point (the turning point) that the photon count suddenly jumps to a very high value. The location of this turning point is characteristic of a specific magnetic order. Hence by locating the turning point we can detect the magnetic phase of the system. Thus our method provides a different way to detect exotic quantum magnetism in ultracold condensates. We would also like to mention that we have only considered the average photon number leaked from the cavity as a method to detect the magnetic order inside the cavity. The method can be easily extended by evaluating quantities like the quadrature measurement, photon number fluctuation, and noise spectra [73] and is capable of detecting more information about the quantum phases of the SOC BEC inside the cavity. We hope this work will be further extended in this direction and will motivate experiments on cavity optomechanics and cavity quantum electrodynamics with SOC cold gases.

However, an important issue related to the detection of all these phases is the energy scale of the effective Hamiltonian which gives rise to such phases, i.e., J^2/U. Hence the temperature required to realize such orders becomes $\sim J$, which is still not achieved with the current cooling techniques. However, the development of new methods of cooling is in progress [74] and the realization of such magnetic orders in ultracold systems is expected. In that context our results provide a very interesting and alternative method for detecting such quantum magnetic phases.

APPENDIX A: FRAME TRANSFORMATION

1. The unitary transformation

We discuss briefly how to arrive from the time-dependent equation (2), to a time-independent equation (3). For this we enter into a rotating frame which induces a unitary transformation $\hat{U}(t) = \exp[i\omega_p t(\hat{\xi}_{11} + \hat{a}^\dagger\hat{a})]$ and then use the Baker-Campbell-Hausdorff lemma to arrive at (3). The lemma reads

$$e^X Y e^{-X} = Y + [X,Y] + \frac{1}{2!}[X,[X,Y]] + \frac{1}{3!}[X,[X,[X,Y]]] + \cdots . \tag{A1}$$

For our case $X = i\omega_p t(\hat{\xi}_{11} + \hat{a}^\dagger\hat{a})$ and $Y = \hat{H}_A + \hat{H}_C + \hat{H}_I$ as obtained in (2). We evaluate the following commutators one by one:

$$\begin{aligned}[X,\hat{H}_A] &= i\omega_p t\left[\hat{\xi}_{11} + \hat{a}^\dagger\hat{a}, \frac{\hat{\mathbf{\Pi}}^2}{2m} + \hbar\omega_{12}\hat{\xi}_{11} + \hbar\omega_{13}\hat{\xi}_{11}\right] \\ &= i\omega_p t\hbar\omega_{12}[\hat{\xi}_{11},\hat{\xi}_{11}] + i\omega_p t\hbar\omega_{13}[\hat{\xi}_{11},\hat{\xi}_{11}] \\ &= 0, \end{aligned} \tag{A2}$$

$$\begin{aligned}[X,\hat{H}_C] &= i\omega_p t\left[\hat{\xi}_{11} + \hat{a}^\dagger\hat{a}, \hbar\omega_c\hat{a}^\dagger\hat{a} - i\hbar\eta\left(\hat{a}e^{i\omega_p t} - \hat{a}^\dagger e^{-i\omega_p t}\right)\right] \\ &= \hbar\eta\omega_p t\left([\hat{a}^\dagger\hat{a},\hat{a}]e^{i\omega_p t} - [\hat{a}^\dagger\hat{a},\hat{a}^\dagger]e^{-i\omega_p t}\right) \\ &= -\hbar\eta\omega_p t\left(\hat{a}e^{i\omega_p t} + \hat{a}^\dagger e^{-i\omega_p t}\right), \end{aligned} \tag{A3}$$

$$[X,\hat{H}_I] = \hbar g(\boldsymbol{x})\omega_p t[\hat{\xi}_{11} + \hat{a}^\dagger\hat{a}, (\hat{\xi}_{12}\hat{a} - \hat{\xi}_{21}\hat{a}^\dagger + \hat{\xi}_{13}\hat{a} - \hat{\xi}_{31}\hat{a}^\dagger)]. \tag{A4}$$

We note the following commutators: $[\hat{\xi}_{11},\hat{\xi}_{12}] = [|1\rangle\langle 1|, |1\rangle\langle 2|] = |1\rangle\langle 2| = \hat{\xi}_{12}$. Similarly, $[\hat{\xi}_{11},\hat{\xi}_{21}] = -\hat{\xi}_{21}$, $[\hat{\xi}_{11},\hat{\xi}_{13}] = \hat{\xi}_{13}$, $[\hat{\xi}_{11},\hat{\xi}_{31}] = -\hat{\xi}_{31}$. Using these, the above equation gets

simplified as

$$[X,\hat{H}_I] = \hbar g(\boldsymbol{x})\omega_p t(\hat{\xi}_{12}\hat{a} + \hat{\xi}_{21}\hat{a}^\dagger + \hat{\xi}_{13}\hat{a} + \hat{\xi}_{31}\hat{a}^\dagger - \hat{\xi}_{12}\hat{a} - \hat{\xi}_{21}\hat{a}^\dagger - \hat{\xi}_{13}\hat{a} - \hat{\xi}_{31}\hat{a}^\dagger) = 0. \quad \text{(A5)}$$

Hence the only nonvanishing commutator is $[X,\hat{H}_C]$. Its higher order commutators can be evaluated similarly, e.g., $[X,[X,\hat{H}_C]] = i\hbar\eta\omega_p^2 t^2(\hat{a}e^{i\omega_p t} - \hat{a}^\dagger e^{-i\omega_p t})$, and so on. Plugging all these commutator values into Baker's lemma, we arrive at Eq. (3).

2. Rederivation of the results without the unitary transformation

The unitary transformation removes the *slow* time dependence of the atom-photon Hamiltonian [Eq. (2)], and the resulting Hamiltonian [Eq. (3)] is obtained in a rotating frame. This makes the rest of the analysis simpler by making it time independent. However, to compare the results in this rotating frame and the laboratory frame, we rederive the important results without performing this unitary transformation and establish consistency between the results of both frames, in the limit of large atom-photon detuning.

The many-body version of Eq. (2) without the transformation would be

$$\hat{\mathcal{H}}_A = \int d\boldsymbol{x}\Big[\hat{\Psi}_2^\dagger(\boldsymbol{x})\Big(\frac{\hat{\boldsymbol{\Pi}}^2}{2m}\Big)\hat{\Psi}_2(\boldsymbol{x}) + \hat{\Psi}_3^\dagger(\boldsymbol{x})\Big(\frac{\hat{\boldsymbol{\Pi}}^2}{2m}\Big)\hat{\Psi}_3(\boldsymbol{x}) + \hat{\Psi}_1^\dagger(\boldsymbol{x})\Big(\frac{\hat{\boldsymbol{\Pi}}^2}{2m} - \hbar\omega_a\Big)\hat{\Psi}_1(\boldsymbol{x})\Big], \quad \text{(A6a)}$$

$$\hat{\mathcal{H}}_I = -i\hbar\int d\boldsymbol{x}[\hat{\Psi}_1^\dagger(\boldsymbol{x})\hat{a}\hat{\Psi}_2(\boldsymbol{x}) + \hat{\Psi}_1^\dagger(\boldsymbol{x})\hat{a}\hat{\Psi}_3(\boldsymbol{x}) + \text{H.c.}]g(\boldsymbol{x}), \quad \text{(A6b)}$$

$$\hat{\mathcal{H}}_U = \frac{U}{2}\int d\boldsymbol{x}[\hat{\Psi}_2^\dagger(\boldsymbol{x})\hat{\Psi}_2^\dagger(\boldsymbol{x})\hat{\Psi}_2(\boldsymbol{x})\hat{\Psi}_2(\boldsymbol{x}) + \hat{\Psi}_3^\dagger(\boldsymbol{x})\hat{\Psi}_3^\dagger(\boldsymbol{x})\hat{\Psi}_3(\boldsymbol{x})\hat{\Psi}_3(\boldsymbol{x}) + \lambda\hat{\Psi}_2^\dagger(\boldsymbol{x})\hat{\Psi}_3^\dagger(\boldsymbol{x})\hat{\Psi}_2(\boldsymbol{x})\hat{\Psi}_3(\boldsymbol{x})], \quad \text{(A6c)}$$

where we define $\omega_a = \omega_{12}^a + \omega_{13}^a$. Now we calculate the Heisenberg equations of evolution for various field operators (say $\hat{A}$), $i\hbar\partial_t\hat{A} = [\hat{A},\hat{\mathcal{H}}]$:

$$\frac{\partial\hat{\Psi}_1(\boldsymbol{x})}{\partial t} = -i\Big(\frac{\hat{\boldsymbol{\Pi}}^2}{2\hbar m} - \omega_a\Big)\hat{\Psi}_1(\boldsymbol{x}) - g(\boldsymbol{x})\hat{a}(\hat{\Psi}_2(\boldsymbol{x}) + \hat{\Psi}_3(\boldsymbol{x})), \quad \text{(A7a)}$$

$$\frac{\partial\hat{\Psi}_2(\boldsymbol{x})}{\partial t} = -i\Big(\frac{\hat{\boldsymbol{\Pi}}^2}{2\hbar m} + \frac{U}{\hbar}\hat{\Psi}_2^\dagger(\boldsymbol{x})\hat{\Psi}_2(\boldsymbol{x}) + \frac{U\lambda}{\hbar}\hat{\Psi}_3^\dagger(\boldsymbol{x})\hat{\Psi}_3(\boldsymbol{x})\Big)\times\hat{\Psi}_2(\boldsymbol{x}) + g(\boldsymbol{x})\hat{a}^\dagger\hat{\Psi}_1(\boldsymbol{x}), \quad \text{(A7b)}$$

$$\frac{\partial\hat{\Psi}_3(\boldsymbol{x})}{\partial t} = -i\Big(\frac{\hat{\boldsymbol{\Pi}}^2}{2\hbar m} + \frac{U}{\hbar}\hat{\Psi}_3^\dagger(\boldsymbol{x})\hat{\Psi}_3(\boldsymbol{x}) + \frac{U\lambda}{\hbar}\hat{\Psi}_2^\dagger(\boldsymbol{x})\hat{\Psi}_2(\boldsymbol{x})\Big)\times\hat{\Psi}_3(\boldsymbol{x}) + g(\boldsymbol{x})\hat{a}^\dagger\hat{\Psi}_1(\boldsymbol{x}), \quad \text{(A7c)}$$

$$\frac{\partial\hat{a}(t)}{\partial t} = -i\omega_c\hat{a}(t) + \eta e^{-i\omega_p t} + \int d\boldsymbol{x}[\hat{\Psi}_2^\dagger(\boldsymbol{x})g(\boldsymbol{x})\hat{\Psi}_1(\boldsymbol{x}) + \hat{\Psi}_3^\dagger(\boldsymbol{x})g(\boldsymbol{x})\hat{\Psi}_1(\boldsymbol{x})]. \quad \text{(A7d)}$$

It may be noted that all the terms that correspond to detuning in Eq. (3) are frequencies now. Also, the pump-field amplitude is modulated as $\eta e^{-i\omega_p t}$. Eliminating the excited state (by assuming adiabaticity), we get

$$\hat{\Psi}_1(\boldsymbol{x}) = -\frac{i}{\omega_a}g(\boldsymbol{x})\hat{a}(t)[\hat{\Psi}_2(\boldsymbol{x}) + \hat{\Psi}_3(\boldsymbol{x})]. \quad \text{(A8)}$$

Replacing this in the above set of equations we get the effective time evolution of the atom and photon operators. The effective Hamiltonian that gives this evolution is

$$\hat{\mathcal{H}}_{\text{eff}}^{(1)} = \int d\boldsymbol{x}\hat{\boldsymbol{\Psi}}^\dagger(\boldsymbol{x})\Big(\frac{\hat{\boldsymbol{\Pi}}^2}{2m} + U_{\text{lat}}\Big)\hat{\boldsymbol{\Psi}}(\boldsymbol{x}) + \hat{H}_c + \frac{1}{2}\int d\boldsymbol{x}\sum_{s,s'}U_{s,s'}\hat{\Psi}_s^\dagger(\boldsymbol{x})\hat{\Psi}_{s'}^\dagger(\boldsymbol{x})\hat{\Psi}_{s'}(\boldsymbol{x})\hat{\Psi}_s(\boldsymbol{x}), \quad \text{(A9)}$$

where $U_{\text{lat}} = V_0[\cos^2(Kx) + \cos^2(Ky)]$. Now we do the tight-binding analysis in Sec. II C, and then to eliminate the photon degrees of freedom, under the bad-cavity limit (see Sec. III A), we get the photon evolution as $\partial_t\hat{a} = \frac{1}{i\hbar}[\hat{a},\hat{H}_{\text{eff}}^{(2)}] = -\hat{D}\hat{a} + \eta e^{-i\omega_p t}$, where $\hat{D} = \kappa + i[U_0(J_0\hat{\mathcal{N}} + J_1\hat{\mathcal{T}}) - \omega_c]$. After eliminating the cavity freedom we get

$$\hat{\mathcal{H}}_{eff}^{(3)} = -\tilde{J}_0\hat{\mathcal{T}} + \tilde{J}_1\hat{\mathcal{T}}^2 + \cdots + \frac{1}{2}\sum_{i,s,s'}U_{s,s'}\hat{b}_{is}^\dagger\hat{b}_{is'}^\dagger\hat{b}_{is'}\hat{b}_{is}, \quad \text{(A10)}$$

$$\tilde{J}_0/J_1 = U_0\eta^2 e^{-2i\omega_p t}\frac{\kappa^2 - \Delta_c'^2}{\left(\kappa^2 + \Delta_c'^2\right)^2} - E/J_1, \quad \text{(A11a)}$$

$$\tilde{J}_1/J_1^2 = 3U_0^2\eta^2 e^{-2i\omega_p t}\Delta_c'\frac{3\kappa^2 - \Delta_c'^2}{\left(\kappa^2 + \Delta_c'^2\right)^4}. \quad \text{(A11b)}$$

Here $\Delta_c' = \omega_c - U_0N_0J_0$. Note that Δ_c in the original case is of the order of ω_c, hence this redefined Δ_c' is also of the same order as the previous Δ_c'. Applying a similar analysis we arrive at

$$n_{\text{ph}} = \langle\hat{a}^{\dagger(s)}\hat{a}^{(s)}\rangle_\Psi = \frac{\eta^2}{\kappa^2 + (\Delta_c' - U_0J_1\langle\hat{\mathcal{T}}\rangle_\Psi)^2}e^{-i\omega_p t}. \quad \text{(A12)}$$

Clearly, in the absence of the unitary transformation the cavity transmission spectrum in the laboratory frame gets an additional oscillatory time-dependent factor compared to the expression given in (30). So by performing the unitary transformation (i.e., by entering in a rotating frame) the above time-dependent factor in Eq. (A12) is removed.

The equivalence between the results obtained with and those without the unitary transformation can be established under the assumption that $\omega_p \ll \omega_a$, i.e., the pump frequency is much higher than the atomic transition frequency. This assumption first enables one to adiabatically eliminate the excited state and, thus, arrive at the effective Hamiltonian in (11). And more importantly, because of this assumption, even if one obtains the expressions in a rotating frame and performs the experiment in the laboratory frame, one observes similar features, provided the observations are done on a time scale which is much shorter compared to this evolution (which can be achieved through a suitable choice of laser detuning). Hence

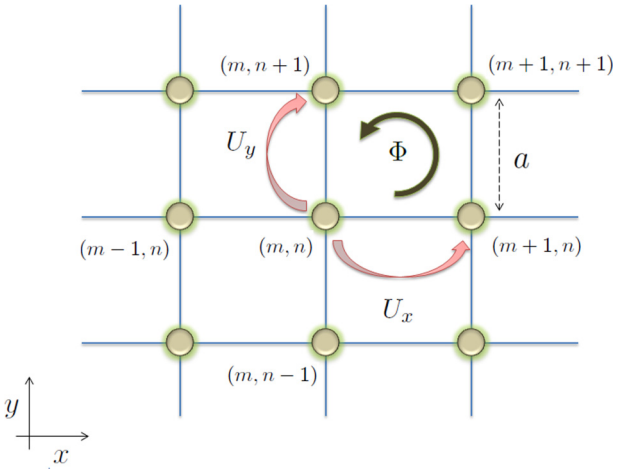

FIG. 7. (Color online) Schematic of an optical lattice. The phase operator U_x determines the phase acquired by an atom when it hops from site (m,n) to site $(m+1,n)$. Similarly, the operator U_y determines the phase acquired by hopping along the positive y axis. The operators $U_x^\dagger$ and $U_y^\dagger$ determine the phase acquired in hopping along the negative x and y axes, respectively.

the the conclusion obtained from the magnetic phases from Eqs. (30) and (A12) will be the same under this approximation.

APPENDIX B: THE HOPPING OPERATOR

In this Appendix we obtain the full form of the hopping operator $\hat{\mathcal{T}}$ in terms of the atom creation (annihilation) operators, $\hat{b}^\dagger_{(m,n)}$ ($\hat{b}_{(m,n)}$). Then we diagonalize it to obtain the spectrum of the tight-binding Hamiltonian, (26). Finally, we show how to evaluate the expectation values of this hopping operator with respect to various magnetic orders.

The lattice sites are indexed as (m,n) and $m,n \in \{0,K-1\}$, which makes the lattice a $K\times K$ one (see Fig. 7). We also use i and j to shorten the notation for (m,n) and (m',n'), respectively. An operator of the form $\hat{b}^\dagger_{\sigma,j}\hat{b}_{\sigma',i}$ creates an atom of pseudospin σ at site j by annihilating an atom of pseud-spin σ' at site i. In Fig. 7 we have shown the action of all possible hopping operators with nontrivial actions. In the presence of a gauge potential, as the particle moves in the lattice potential its wave function acquires a geometric phase as a result of the Aharonov-Bohm effect. The phase acquired by an atom upon hopping from site $\boldsymbol{r}_i$ to site $\boldsymbol{r}_j$, ϕ_{ij}, is given by

$$\phi_{ij} = \int_{\boldsymbol{r}_i}^{\boldsymbol{r}_j} \boldsymbol{A}(\boldsymbol{r}')\cdot d\boldsymbol{l} = \alpha\sigma_y(x_j - x_i) + \beta\sigma_x(y_j - y_i) + \mathbb{1}B_0 x_i(y_j - y_i). \tag{B1}$$

For hopping along the x axis, i.e., $m \to m\pm 1$, the phase acquired is $\phi_x = \alpha\sigma_y(x_{i+1} - x_i) + 0 = \alpha\sigma_y$, and for hopping along the y axis, i.e., $n \to n\pm 1$, it is $\phi_y = 0 + (\beta\sigma_x + B_0 x_i)(y_{i+1} - y_i) = (-\beta\sigma_x + \mathbb{1}B_0 x)$.

An alternative way to discuss this is to define a set of unitary operators along the x and y axes which, when acting on the wave function, would produce nontrivial phases. These gauge-potential-dependent phase operators are

$$U_x = e^{-i\phi_x}, \quad U_y = e^{-i\phi_y}. \tag{B2}$$

With our particular choice of vector potential, i.e., $\boldsymbol{A} = (\alpha\sigma_y, \beta\sigma_x + 2\pi\Phi m, 0)$, one can calculate the phase operators as

$$U_x = \begin{pmatrix} \cos\alpha & -\sin\alpha \\ \sin\alpha & \cos\alpha \end{pmatrix},$$
$$U_y = e^{-i2\pi\Phi m}\begin{pmatrix} \cos\beta & -i\sin\beta \\ i\sin\beta & \cos\beta \end{pmatrix}. \tag{B3}$$

Thus a generic form of the tunneling operator $\hat{\mathcal{T}}$ (for a 2D lattice) can now be written as

$$\hat{\mathcal{T}} = \sum_{m,n} \hat{b}^\dagger_{m+1} U_x \hat{b}_m + \hat{b}^\dagger_{n+1} U_y \hat{b}_n + \text{H.c.} \tag{B4}$$

Here we have denoted $\hat{b}^\dagger_m$ for $(\hat{b}^\dagger_{m,\uparrow}\ \hat{b}^\dagger_{m,\downarrow})$, and similarly, $\hat{b}^\dagger_n$ for $(\hat{b}^\dagger_{n,\uparrow}\ \hat{b}^\dagger_{n,\downarrow})$. For our choice of gauge potential we can simplify this equation to

$$\hat{\mathcal{T}} = \sum_{i=x,y} \hat{\mathcal{T}}_i^D + \hat{\mathcal{T}}_i^{\text{ND}},$$
$$\hat{\mathcal{T}}_y^D = \cos\beta \sum_n (\hat{b}^\dagger_{n+1,\uparrow}\hat{b}_{n,\uparrow} + \hat{b}^\dagger_{n+1,\downarrow}\hat{b}_{n,\downarrow})e^{-i2\pi\Phi m} + \text{H.c.},$$
$$\hat{\mathcal{T}}_y^{\text{ND}} = -i\sin\beta \sum_n (\hat{b}^\dagger_{n+1,\downarrow}\hat{b}_{n,\uparrow} + \hat{b}^\dagger_{n+1,\uparrow}\hat{b}_{n,\downarrow})e^{-i2\pi\Phi m} + \text{H.c.},$$
$$\hat{\mathcal{T}}_x^D = \cos\alpha \sum_m \hat{b}^\dagger_{m+1,\uparrow}\hat{b}_{m,\uparrow} + \hat{b}^\dagger_{m+1,\downarrow}\hat{b}_{m,\downarrow} + \text{H.c.},$$
$$\hat{\mathcal{T}}_x^{\text{ND}} = \sin\alpha \sum_m \hat{b}^\dagger_{m+1,\downarrow}\hat{b}_{m,\uparrow} - \hat{b}^\dagger_{m+1,\uparrow}\hat{b}_{m,\downarrow} + \text{H.c.} \tag{B5}$$

Here the operator is separated into diagonal ($\hat{\mathcal{T}}_i^D$) and off-diagonal ($\hat{\mathcal{T}}_i^{\text{ND}}$) parts and then each of these parts is written for both the x and the y axes, considering only nearest-neighbor interactions. The off-diagonal terms in the tunneling operator arise because of the spin-orbit coupling. We note that the above tunneling matrix can be diagonalized or the spin-orbit coupling can be eliminated just by a site-dependent rotation. For instance, the following rotation around the x axis at site i diagonalizes the x-axis tunneling operator by removing the spin-orbit coupling:

$$\begin{pmatrix} \hat{b}_{i,\uparrow} \\ \hat{b}_{i,\downarrow} \end{pmatrix} = \begin{pmatrix} \cos\theta_i & -\sin\theta_i \\ \sin\theta_i & \cos\theta_i \end{pmatrix}\begin{pmatrix} \hat{b}'_{i,\uparrow} \\ \hat{b}'_{i,\downarrow} \end{pmatrix}. \tag{B6}$$

Here $\theta_{i+1} - \theta_i = \alpha - \pi/2$. So switching on spin-orbit coupling is equivalent to rotating site i about the x axis by an angle $-\theta_i$, and along with that, the hopping amplitude is also renormalized to $J_1\cos\alpha$.

1. Diagonalization

The Hamiltonian in the momentum space can be written as $\hat{H} = \sum_{\boldsymbol{k}} \hat{\Phi}^\dagger_{\boldsymbol{k}} \hat{H}_{\boldsymbol{k}} \hat{\Phi}_{\boldsymbol{k}}$, where $\hat{\Phi}_k = (\hat{b}_{\uparrow\boldsymbol{k}}, \hat{b}_{\downarrow\boldsymbol{k}})^T$ is the momentum-space representation of the two-component spinor and the atomic operators are also written in the

momentum-space representation:

$$\hat{b}_s(\boldsymbol{r}) = \frac{1}{\sqrt{N_0}}\sum_{\boldsymbol{k}} e^{i\boldsymbol{k}\cdot\boldsymbol{r}}\hat{b}_{s\boldsymbol{k}}, \hat{b}_s^\dagger(\boldsymbol{r}) = \frac{1}{\sqrt{N_0}}\sum_{\boldsymbol{k}} e^{-i\boldsymbol{k}\cdot\boldsymbol{r}}\hat{b}_{s\boldsymbol{k}}^\dagger. \quad \text{(B7)}$$

Writing the atomic operators in the momentum basis we can diagonalize the Hamiltonian (without the interaction part) obtained in (26):

$$\hat{H} = -\tilde{J}_0\sum_s\sum_{\langle m,n\rangle}\frac{1}{N}\sum_{\boldsymbol{k},\boldsymbol{k}'}\hat{b}_{s\boldsymbol{k}}^\dagger(e^{ik_x}e^{-i\sigma_y\alpha} + e^{ik_y}e^{-i2\pi\Phi m}e^{i\sigma_x\alpha})\hat{b}_{s\boldsymbol{k}'} + \text{H.c.} \quad \text{(B8)}$$

Now we invoke orthonormality of the plane-wave basis, $\frac{1}{N}\sum_{\boldsymbol{r}} e^{-i\boldsymbol{r}\cdot(\boldsymbol{k}-\boldsymbol{k}')} = \delta(\boldsymbol{k}-\boldsymbol{k}')$, and Euler's identity, $\exp[i\theta(\hat{n}\cdot\vec{\sigma})] = \mathbf{1}\cos\theta + i(\hat{n}\cdot\vec{\sigma})\sin\theta$, and denoting $\epsilon_m = k_y - 2\pi m\Phi$ we obtain

$$\hat{H}_k = \cos\alpha(\cos\epsilon_m + \cos k_x)\mathbf{1} - \sin\alpha(\sin\epsilon_m\sigma_x - \iota\sin k_x\sigma_y). \quad \text{(B9)}$$

Using the 2×2 representation of the Pauli matrices we obtain a 2×2 Hamiltonian. Writing this Hamiltonian in its eigenbasis we diagonalize it. Thus the spectrum is

$$E_\pm = 2\cos\alpha(\cos\epsilon_m + \cos k_x) \pm 2\sin\alpha\sqrt{\sin^2\epsilon_m + \sin^2 k_x}. \quad \text{(B10)}$$

2. Expectation values

In this section we calculate $\langle\Psi_{\rm MI}|\hat{\mathcal{T}}|\Psi_{\rm MI}\rangle$, which appears in Eq. (30). The full form of $\hat{\mathcal{T}}$ is obtained in (B5). We assume that there are exactly equal numbers of lattices in the A and B sublattices, hence the total number of lattice sites is even, i.e., $N_0 = K^2$ is even. We demonstrate the calculation for a simple 2×2 site problem and then generalize it for multiple sites. In this case the MI wave function becomes

$$|\Psi_{\rm MI}\rangle = |\psi_A\rangle_{00}|\psi_B\rangle_{01}|\psi_A\rangle_{11}|\psi_B\rangle_{10}. \quad \text{(B11)}$$

The bottom-left site is used as the origin of the coordinate system and $(m,n) = (0,0)$ is shortened to 00; other sites are indexed similarly. Here $|\psi_{A,B}\rangle = \cos\frac{\theta_{A,B}}{2}|\uparrow\rangle + e^{i\phi_{A,B}}\sin\frac{\theta_{A,B}}{2}|\downarrow\rangle$. When the operator $\hat{b}_{m+1,\uparrow}^\dagger\hat{b}_{m,\uparrow}$ (fixing $n=1$) acts on the above wave, then (say, $m=1$) it hops a ↑ spin from site m (=1) to $m+1$ (=0). Thus the resulting wave function becomes

$$\hat{b}_{m+1,\uparrow}^\dagger\hat{b}_{m,\uparrow}|\Psi_{\rm MI}\rangle = |\psi_A\rangle_{00}\left(\cos\frac{\theta_B}{2}|\uparrow,\uparrow\rangle + e^{i\phi_B}\sin\frac{\theta_B}{2}|\downarrow\rangle\right)_{01} \times\left(\cos\frac{\theta_A}{2}|0\rangle + e^{i\phi_A}\sin\frac{\theta_A}{2}|\downarrow\rangle\right)_{11}|\psi_B\rangle_{10}. \quad \text{(B12)}$$

Here $|0\rangle$ denotes the spin vacuum. When $\langle\Psi_{\rm MI}|$ acts on the left side of the above expression we obtain

$$\langle\Psi_{\rm MI}|\hat{b}_{m+1,\uparrow}^\dagger\hat{b}_{m,\uparrow}|\Psi_{\rm MI}\rangle = \langle\psi_A|\psi_A\rangle\left(0+\sin^2\frac{\theta_B}{2}\right)\left(0+\sin^2\frac{\theta_A}{2}\right)\langle\psi_B|\psi_B\rangle = \sin^2\frac{\theta_A}{2}\sin^2\frac{\theta_B}{2}. \quad \text{(B13)}$$

The Hermitian conjugate of this operator hops ↑ from $m+1$ to m. Thus $\langle\Psi_{\rm MI}|(\hat{b}_{m+1,\uparrow}^\dagger\hat{b}_{m,\uparrow} + \text{H.c.})|\Psi_{\rm MI}\rangle = 2\sin^2\frac{\theta_B}{2}\sin^2\frac{\theta_A}{2}$. In a similar way we can obtain

$$\langle\Psi_{\rm MI}|\hat{b}_{m+1,\downarrow}^\dagger\hat{b}_{m,\downarrow}|\Psi_{\rm MI}\rangle = \cos^2\frac{\theta_A}{2}\cos^2\frac{\theta_B}{2}. \quad \text{(B14)}$$

The action of the hopping operator which involves spin flip can be obtained as

$$\hat{b}_{m+1,\downarrow}^\dagger\hat{b}_{m,\uparrow}|\Psi_{\rm MI}\rangle = |\psi_A\rangle_{00}\left(\cos\frac{\theta_B}{2}|\uparrow\rangle + e^{i\phi_B}\sin\frac{\theta_B}{2}|\downarrow,\uparrow\rangle\right)_{01} \times\left(\cos\frac{\theta_A}{2}|0\rangle + e^{i\phi_A}\sin\frac{\theta_A}{2}|\downarrow\rangle\right)_{11}|\psi_B\rangle_{10} = 0. \quad \text{(B15)}$$

So terms like $\hat{b}_{m+1,\downarrow}^\dagger\hat{b}_{m,\uparrow}$ and $\hat{b}_{m+1,\uparrow}^\dagger\hat{b}_{m,\downarrow}$ do not contribute to the expectation. When we have a $K\times K$ lattice there will be $K-1$ hoppings possible along the x axis, yielding a contribution of $2(K-1)\cos^2\frac{\theta_A}{2}\cos^2\frac{\theta_B}{2} + \sin^2\frac{\theta_B}{2}\sin^2\frac{\theta_A}{2}$. There are K such x axes so total contribution becomes

$$\langle\hat{\mathcal{T}}_x\rangle = 2\cos\alpha K(K-1)\left[\sin^2\frac{\theta_A}{2}\sin^2\frac{\theta_B}{2} + \cos^2\frac{\theta_A}{2}\cos^2\frac{\theta_B}{2}\right]. \quad \text{(B16)}$$

Now we turn to hopping along the y axis. We switch on the Abelian gauge field discussed in the text; see Eq. (B5) for the full form of the Hopping operator. Hence now each hopping along the y-axis is associated with a phase depending on the x-axis coordinate of the site, i.e., $e^{-2\pi i\Phi m}$. For hopping along negative y-axis, the associated phase factor is $e^{+2\pi i\Phi m}$. Using a similar argument we arrive at the following result:

$$\langle\hat{\mathcal{T}}_y\rangle = 2\cos\beta(K-1)\sum_{m=0}^{K-1}\cos(2\pi m\Phi) \times\left[\sin^2\frac{\theta_A}{2}\sin^2\frac{\theta_B}{2} + \cos^2\frac{\theta_A}{2}\cos^2\frac{\theta_B}{2}\right]. \quad \text{(B17)}$$

The latter expression can be simplified to $f(K,\Phi) = \sum_{m=0}^{K-1}\cos(2\pi m\Phi) = \frac{\sin(K\pi\Phi)}{\sin(\pi\Phi)}\cos[\pi\Phi(K-1)]$. Thus the full expectation becomes

$$\langle\hat{\mathcal{T}}\rangle = 2\cos\alpha(K-1)[\cos\alpha K + \cos\beta f(K,\Phi)] \times\left[\sin^2\frac{\theta_A}{2}\sin^2\frac{\theta_B}{2} + \cos^2\frac{\theta_A}{2}\cos^2\frac{\theta_B}{2}\right]. \quad \text{(B18)}$$

[1] I. Bloch, J. Dalibard, and S. Naschimbene, Nat. Phys. Insight **8**, 267 (2012).

[2] I. Bloch, J. Dalibard, and W. Zwerger, Rev. Mod. Phys. **80**, 885 (2008).

[3] M. Lewenstein, A. Sanpera, and V. Ahufinger, *Ultracold Atoms in Optical Lattices: Simulating Quantum Many-Body Systems* (Oxford University Press, Oxford, 2012).

[4] Y.-J. Lin, K. Jiménez-Garcia, and I. B. Spielman, Nature (London) **471**, 83 (2011).

[5] J. Dalibard, F. Gerbier, G. Juzeliünas, and P. Ohberg, Rev. Mod. Phys. **83**, 1523 (2011); J. Radić, T. A. Sedrakyan, I. B. Spielman, and V. Galitski, Phys. Rev. A **84**, 063604 (2011).

[6] L. W. Cheuk, A. T. Sommer, Z. Hadzibabic, T. Yefsah, W. S. Bakr, and M. W. Zwierlein, Phys. Rev. Lett. **109**, 095302 (2012).

[7] P. Wang, Z.-Q. Yu, Z. Fu, J. Miao, L. Huang, S. Chai, H. Zhai, and J. Zhang, Phys. Rev. Lett. **109**, 095301 (2012).

[8] M. Z. Hassan and C. L. Cane, Rev. Mod. Phys. **82**, 3045 (2010); T. A. Sedrakyan, A. Kamenev, and L. I. Glazman, Phys. Rev. A **86**, 063639 (2012).

[9] A. Auerbach, *Interacting Electrons and Quantum Magnetism* (Springer-Verlag, Berlin, 1998).

[10] V. Galitski and I. B. Spielman, Nature **494**, 49 (2013).

[11] H. Ritsch, P. Domokos, F. Brennecke, and T. Esslinger, Rev. Mod. Phys. **85**, 553 (2013).

[12] A. Öttl, S. Ritter, M. Köhl, and T. Esslinger, Phys. Rev. Lett. **95**, 090404 (2005).

[13] F. Brennecke, T. Donner, S. Ritter, T. Bourdel, M. Köhl, and T. Esslinger, Nature (London) **450**, 268 (2007).

[14] K. W. Murch, K. L. Moore, S. Gupta, D. M. Stamper Kurn, Nat. Phys. **4**, 561 (2008).

[15] S. Slama, S. Bux, Krenz, C. Zimmermann, P. W. Courteille, Phys. Rev. Lett. **98**, 053603 (2007).

[16] I. B. Mekhov, C. Maschler, and H. Ritsch, Nat. Phys. **3**, 319 (2007).

[17] I. B. Mekhov and H. Ritsch, Phys. Rev. Lett. **102**, 020403 (2009);Phys. Rev. A **80**, 013604 (2009).

[18] S. Gopalakrishnan, B. L. Lev, and P. M. Goldbart, Nat. Phys. **5**, 845 (2009).

[19] P. Domokos and H. Ritsch, Phys. Rev. Lett. **89**, 253003 (2002); J. K. Asbóth, P. Domokos, H. Ritsch, and A. Vukics, Phys. Rev. A **72**, 053417 (2005).

[20] P. Münstermann, T. Fischer, P. Maunz, P. W. H. Pinkse, and G. Rempe, Phys. Rev. Lett. **84**, 4068 (2000).

[21] R. Mottl, F. Brennecke, K. Baumann, R. Landig, T. Donner, and T. Esslinger, Science **336**, 1570 (2012).

[22] W. Chen, K. Zhang, D. S. Goldbaum, M. Bhattacharya, and P. Meystre, Phys. Rev. A **80**, 011801(R) (2009).

[23] C. Maschler and H. Ritsch, Phys. Rev. Lett. **95**, 260401 (2005).

[24] D. Jaksch, C. Bruder, J. I. Cirac, C. W. Gardiner, and P. Zoller, Phys. Rev. Lett. **81**, 3108 (1998).

[25] M. Greiner, M. O. Mandel, T. Esslinger, T. Hänsch, and I. Bloch, Nature **415**, 39 (2002).

[26] W. S. Cole, S. Zhang, A. Paramekanti, and N. Trivedi, Phys. Rev. Lett. **109**, 085302 (2012).

[27] S. Mandal, K. Saha, and K. Sengupta, Phys. Rev. B **86**, 155101 (2012).

[28] J. Radić, A. Di Ciolo, K. Sun, and V. Galitski, Phys. Rev. Lett. **109**, 085303 (2012).

[29] Z. Cai, X. Zhou, and C. Wu, Phys. Rev. A **85**, 061605(R) (2012).

[30] B. Padhi and S. Ghosh, Phys. Rev. Lett. **111**, 043603 (2013).

[31] L. P. Guo, L. Du, and Y. Zhang, Eur. Phys. J. D **55**, 531 (2009).

[32] F. Mivehvar and D. L. Feder, Phys. Rev. A **89**, 013803 (2014).

[33] B. Estienne, S. M. Haaker, and K. Schoutens, New J. Phys. **13**, 045012 (2011).

[34] M. E. Peshkin and D. V. Schroeder, *An Introduction to Quantum Field Theory*, 1st ed. (Levant Books, Kolkata, India, 2005).

[35] E. Jaynes and F. Cummings, Proc. IEEE **51**, 89 (1963).

[36] Y. J. Lin, R. L. Compton, K. Jimnez-Garca, J. V. Porto, and I. B. Spielman, Nature **462**, 628 (2009).

[37] Y. A. Bychkov and E. I. Rashba, J. Phys. C **17**, 6039 (1984); G. Dresselhaus, Phys. Rev. **100**, 580 (1955).

[38] C. Maschler, I. B. Mekhov, and H. Ritsch, Eur. Phys. J. D **46**, 545 (2008).

[39] C. W. Gardiner and P. Zoller, *Quantum Noise*, 3rd ed. (Springer, New Delhi, 2005).

[40] M. Aspelmeyer, T. J. Kippenberg, and F. Marquardt, arXiv:1303.0733.

[41] C. Kittel, *Quantum Theory of Solids* (John Wiley & Sons, New York, 1963).

[42] Y. Deng, J. Cheng, H. Jing, and S. Yi, Phys. Rev. Lett. **112**, 143007 (2014).

[43] K. Baumann, C. Guerlin, F. Brennecke, and T. Esslinger, Nature (London) **464**, 1301 (2010).

[44] P. Strack and S. Sachdev, Phys. Rev. Lett. **107**, 277202 (2011).

[45] C. Chin, R. Grimm, P. Julienne, and E. Tiesinga, Rev. Mod. Phys. **82**, 1225 (2010), and references therein.

[46] N. R. Claussen, S. J. J. M. F. Kokkelmans, S. T. Thompson, E. A. Donley, E. Hodby, and C. E. Wieman, Phys. Rev. A **67**, 060701(R) (2003).

[47] A. Marte, T. Volz, J. Schuster, S. Dürr, G. Rempe, E. G. M. van Kempen, and B. J. Verhaar, Phys. Rev. Lett. **89**, 283202 (2002); T. Volz, S. Dürr, S. Ernst, A. Marte, and G. Rempe, Phys. Rev. A **68**, 010702(R) (2003).

[48] M. Theis, G. Thalhammer, K. Winkler, M. Hellwig, G. Ruff, R. Grimm, and J. H. Denschlag, Phys. Rev. Lett. **93**, 123001 (2004).

[49] G. Thalhammer, M. Theis, K. Winkler, R. Grimm, and J. H. Denschlag, Phys. Rev. A **71**, 033403 (2005).

[50] D. R. Hofstadter, Phys. Rev. B **14**, 2239 (1976).

[51] M. Aidelsburger, M. Atala, M. Lohse, J. T. Barreiro, B. Paredes, and I. Bloch, Phys. Rev. Lett. **111**, 185301 (2013); H. Miyake, G. A. Siviloglou, C. J. Kennedy, W. C. Burton, and W. Ketterle, *ibid.* **111**, 185302 (2013).

[52] N. Goldman, A. Kubasiak, P. Gaspard, and M. Lewenstein, Phys. Rev. A **79**, 023624 (2009).

[53] B. P. Anderson and M. A. Kasevich, Science **282**, 1686 (1998); L. Tarruell, D. Greif, T. Uehlinger, G. Jotzu, and T. Esslinger, Nature (London) **483**, 302 (2012).

[54] S. Ashhab and A. J. Leggett, Phys. Rev. A **68**, 063612 (2003).

[55] S.-L. Zhu, B. Wang, and L.-M. Duan, Phys. Rev. Lett. **98**, 260402 (2007).

[56] G. Montambaux, F. Piéchon, J.-N. Fuchs, and M. O. Goerbig, Phys. Rev. B **80**, 153412 (2009); L.-K. Lim, J. N. Fuchs, and G. Montambaux, Phys. Rev. Lett. **108**, 175303 (2012); K. K. Gomes, W. Mar, W. Ko, F. Guinea, and H. C. Manoharan, Nature (London) **483**, 306 (2012).

[57] Z. Chen and B. Wu, Phys. Rev. Lett. **107**, 065301 (2011); L. Wang and L. Fu, Phys. Rev. A **87**, 053612 (2013).

[58] E. Altman, W. Hofstetter, E. Demler, and M. D. Lukin, New J. Phys. **5**, 113 (2003).

[59] A. B. Kuklov and B. V. Svistunov, Phys. Rev. Lett. **90**, 100401 (2003); A. Kuklov, N. Prokofev, and B. Svistunov, *ibid.* **92**, 050402 (2004).
[60] L.-M. Duan, E. Demler, and M. D. Lukin, Phys. Rev. Lett. **91**, 090402 (2003).
[61] I. Dzyaloshinskii, J. Phys. Chem. Solids **4**, 241 (1958); T. Moriya, Phys. Rev. **120**, 91 (1960).
[62] J. Larson, B. Damski, G. Morigi, and M. Lewenstein, Phys. Rev. Lett. **100**, 050401 (2008).
[63] P. Meystre and M. Sargent III, *Elements of Quantum Optics*, 3rd ed. (Springer, New Delhi, 2009).
[64] M. P. A. Fisher, P. B. Weichman, G. Grinstein, and D. S. Fisher, Phys. Rev. B **40**, 546 (1989).
[65] K. Sheshadri, H. R. Krishnamurty, R. Pandit, and T. V. Ramkrishnan, Europhys. Lett. **22**, 257 (1993); L. Amico and V. Penna, Phys. Rev. Lett. **80**, 2189 (1998).
[66] T. Grass, K. Saha, K. Sengupta, and M. Lewenstein, Phys. Rev. A **84**, 053632 (2011).
[67] T. A. Corcovilos, S. K. Baur, J. M. Hitchcock, E. J. Mueller, and R. G. Hulet, Phys. Rev. A **81**, 013415 (2010).
[68] E. Altman, E. Demler, and M. D. Lukin, Phys. Rev. A **70**, 013603 (2004).
[69] J. M. Higbie, L. E. Sadler, S. Inouye, A. P. Chikkatur, S. R. Leslie, K. L. Moore, V. Savalli, and D. M. Stamper-Kurn, Phys. Rev. Lett. **95**, 050401 (2005).
[70] K. D. Nelson, X. Li, and D. S. Weiss, Nat. Phys. **3**, 556 (2007).
[71] A. Isacsson, M.-C. Cha, K. Sengupta, and S. M. Girvin, Phys. Rev. B **72**, 184507 (2005).
[72] A. Agarwala, M. Nath, J. Lugani, K. Thyagarajan, and S. Ghosh, Phys. Rev. A **85**, 063606 (2012).
[73] D. C. McKay and B. DeMarco, Rep. Prog. Phys. **74**, 054401 (2011); C. J. M. Mathy, D. A. Huse, and R. G. Hulet, Phys. Rev. A **86**, 023606 (2012).
[74] I. B. Mekhov, C. Mashler, and H. Ritsch, Phys. Rev. A **76**, 053618 (2007).